Wind and ACE observations during the great flow of 1–4 May 1998: Relation to solar activity and implications for the magnetosphere

C. J. Farrugia,[1] M. Popecki,[1] E. Möbius,[1] V. K. Jordanova,[1] M. I. Desai,[2] R. J. Fitzenreiter,[3] K. W. Ogilvie,[3] H. Matsui,[1] S. Lepri,[4] T. Zurbuchen,[4] G. M. Mason,[2,5] G. R. Lawrence,[3,6] L. F. Burlaga,[3] R. P. Lepping,[3] J. R. Dwyer,[7] and D. McComas[8]

Received 22 June 2001; revised 2 December 2001; accepted 7 December 2001; published 14 September 2002.

[1] Using magnetic field, plasma, and energetic particle data from Wind and ACE, we analyze interplanetary features associated with the first strongly geoeffective interval in the rising phase of solar cycle 23, which affected Earth on 1–4 May 1998. As shown by *Skoug et al.* [1999], the configuration consisted of a compound stream made up of an interplanetary coronal mass ejection (ICME) containing a magnetic cloud and being trailed by a hot, faster flow. In addition, we find that the front boundary of the ICME is a rotational discontinuity and the leading edge of the fast stream has a zero normal magnetic field component and is followed by a magnetic field which is strongly enhanced (by a factor of ~4) and whose fluctuations lie in a plane approximately parallel to the leading edge. Energetic particle and composition observations confirm that the field lines of the magnetic cloud were connected to at least two different flare sites in the same active region. We infer a lower limit for the size of the solar footprint of the connected flux tube of 0.02 R_S^2, i.e., $\sim 10^{10}$ km^2. A dramatic weakening of the halo electron distribution occurred during 3 May at the time when other experimenters have documented the presence of prominence material. We hypothesize that the solar wind halo population was scattered by enhanced frequency of Coulomb collisions in the dense and very cold plasma. We discuss our energetic particle observations in terms of local acceleration at interplanetary shocks and field discontinuities as well as in terms of acceleration in flares and CME-driven shocks. We also compare, in a specific formulation, the power and energy input of the May 1998 configuration to the magnetosphere with other much studied geoeffective events. We find that the power input far exceeded that in all previous geoeffective events in our sample and attribute this to the fact that the 1–4 May 1998 event consisted of a compound stream structure with an unprecedented power input during a ~3-hour burst of high-speed flow on 4 May. A statistical survey using the OMNI database for the 6-year period 1995–2000 confirms these inferences and indicates further approximate saturation levels for energy and power input of 10 J m^{-2} and 0.3 mW m^{-2}, only exceeded in exceptional events such as May 1998 and July 2000. The solar energetic particle event at the leading edge of the fast stream might be the only advance warning the Earth would receive of the approach of a configuration of such a concentrated geoeffective potential. *INDEX TERMS:* 2111 Interplanetary Physics: Ejecta, driver gases, and magnetic clouds; 2118 Interplanetary Physics: Energetic particles, solar; 2139 Interplanetary Physics: Interplanetary shocks; 2784 Magnetospheric Physics: Solar wind/magnetosphere interactions; *KEYWORDS:* magnetic clouds, solar energetic particles, composition, size of solar footprint of connected flux rope, space weather

Citation: Farrugia, C. J., M. Popecki, E. Möbius, V. K. Jordanova, M. I. Desai, R. J. Fitzenreiter, K. W. Ogilvie, H. Matsui, S. Lepri, T. Zurbuchen, G. M. Mason, G. R. Lawrence, L. F. Burlaga, R. P. Lepping, J. R. Dwyer, and D. McComas, Wind and ACE observations during the great flow of 1–4 May 1998: Relation to solar activity and implications for the magnetosphere, *J. Geophys. Res.*, *107*(A9), 1240, doi:10.1029/2001JA000188, 2002.

[1]Space Science Center, University of New Hampshire, Durham, New Hampshire, USA.
[2]Department of Physics, University of Maryland, College Park, Maryland, USA.
[3]NASA Goddard Space Flight Center, Greenbelt, Maryland, USA.
[4]Space Research Building, University of Michigan, Ann Arbor, Michigan, USA.
[5]Also at Institute for Physical Sciences and Technology, University of Maryland, College Park, Maryland, USA.
[6]Department of Physics and Astrophysics, University of Birmingham, UK.
[7]Physics and Space Sciences Department, Florida Institute of Technology, Melbourne, Florida, USA.
[8]Southwest Research Institute, San Antonio, Texas, USA.

0148-0227/02/2001JA000188

1. Introduction

[2] Much interest attaches to observations of the active Sun and signatures of solar activity in interplanetary space, for example, under NASA's Solmax program. The diverse instrumentations on the spacecraft Wind, ACE, and SOHO are providing the most comprehensive data coverage of any solar cycle to date at an unsurpassed temporal resolution. Properly systematized, in both case event as well as statistical studies, this information combined with that acquired near the last solar minimum within the International Solar Terrestrial Physics (ISTP) program would shed light not only on the various forms of solar disturbances as a function of the phase of the solar cycle but also on the chain of causal relations linking solar activity with diverse magnetospheric disturbances. Applications to a reliable space weather predictive tool are an obvious corollary.

[3] Studies over previous solar cycles, mainly during solar cycle 21 when the ISEE 3 spacecraft was in orbit around the L1 Lagrangian point (1978–1982) have shown that around solar cycle maximum interplanetary manifestations of coronal mass ejections (ICMEs) and magnetic clouds (referred to below collectively as ''solar ejecta'') play an overriding role in eliciting a strong geomagnetic response [e.g., *Tsurutani et al.*, 1988; *Zhang and Burlaga*, 1988; *Gosling et al.*, 1990, 1991; *Richardson et al.*, 2000; *Gosling*, 1990; *Tsurutani and Gonzalez*, 1997; *Farrugia et al.*, 1997]. Past work has further highlighted the geoeffective potential of compound streams made up of a solar ejecta interacting with a trailing, faster flow [*Burlaga et al.*, 1987]. It follows that in considering the severity of geomagnetic effects elicited in the magnetosphere we need to consider not only isolated ICMEs and magnetic clouds but also how they evolve and the interplanetary configurations, discontinuities, and flows that they encounter en route to Earth.

[4] This paper deals with a compound stream during the first prolonged active phase of the current solar cycle during the period 20 April 20 to 9 May 1998. During this interval, NOAA's GOES spacecraft recorded a total of 141 X-ray flares, while through its nested white-light coronagraphs, SOHO/LASCO observed 41 coronal mass ejections (CMEs). Of the GOES flares, 16 were M class or greater; 4 of these were X class. From the 16 highest-energy events, only three flares cannot be associated with CMEs, while one other immediately precedes a LASCO data gap. The greater part of this activity seems to be associated with two active regions, AR8210 and AR8214. During 23 April to 2 May 1998, when one or both of these active regions were closest to the solar disk center, six ''halo'' CMEs (where ejected mass is visible around all 360° of LASCO's occulting disk) were observed, and a further four events displaying >180° coverage were seen prior to, or after, this period. Such events are indicative of a solar ejecta propagating toward Earth, and their abundance during this period provides many possible drivers for the very disturbed conditions prevailing in the magnetosphere.

[5] In two papers we shall characterize in a case study the interplanetary conditions during the 4-day period 1–4 May 1998, from data returned by various instruments on Wind and ACE (this paper), and investigate the global geomagnetic disturbances caused inside the magnetosphere (C. Farrugia et al., manuscript in preparation, 2002). In particular, we analyze the magnetic field, solar wind plasma, energetic protons and electrons, and energetic elemental and ionic composition from Wind and ACE during this period. We use data from the following instruments: the Magnetic Field Investigation (MFI) [*Lepping et al.*, 1995], the Solar Wind Experiment (SWE) [*Ogilvie et al.*, 1995], and the Three-Dimensional Plasma and Energetic Particle Investigation [*Lin et al.*, 1995] on the Wind spacecraft; the Energetic Particles Acceleration, Composition, and Transport (EPACT) Investigation on Wind [*von Rosenvinge et al.*, 1995]; the Electron, Proton and Alpha Monitor (EPAM) [*Gold et al.*, 1998], the Solar Energetic Particle Ionic Charge Analyzer (SEPICA) [*Möbius et al.*, 1998], and the Solar Wind Ion Composition Spectrometer on the ACE spacecraft (SWICS) [*Gloeckler et al.*, 1998]. Various aspects of the interplanetary observations during this period have been discussed in other papers [*Gloeckler et al.*, 1999; *Skoug et al.*, 1999; *Klecker et al.*, 2000; *Popecki et al.*, 2000]. However, we shall here add more information and analysis as regards the nature of the discontinuities present, using the behavior of the energetic particles and ionic and elemental composition with respect to these boundaries for the first time, and probe the magnetic connection of the solar ejecta to active regions on the Sun.

[6] We find the interplanetary medium to consist of a complex compound stream where a number of discontinuities/shocks played an important role in particle energization. At the ''core'' of the compound stream is a magnetic cloud [*Burlaga et al.*, 1981] where a large and smooth rotation of the magnetic field vector takes place in a cold magnetoplasma of enhanced field strength. Energetic particle and charge-state measurements show that the magnetic cloud retained magnetic connection to various flare sites within the same active region on the Sun. From this, a lower limit to the size of the solar footprint of the ejection is derived. In the later portion of the magnetic cloud passage over Wind on 3 May an extremely weak solar wind halo is observed. This may either be due to disconnection of magnetic field lines from the Sun or to the fact that the plasma is too cold to have significant count rate above the SWE instrumental threshold (13 eV, see below), or to scattering of the halo by Coulomb collisions. We think the latter possibility is the most plausible partly because extremely high densities and low proton temperatures were measured on 3 May and partly because continued magnetic connection offers a natural explanation for bursty enhancements of iron charge states observed on 3 May.

[7] We then consider power input to the magnetosphere, calculated in the ''epsilon parameter'' formulation of *Perreault and Akasofu* [1978]. The ϵ parameter has been widely and successfully used to relate potential interplanetary power input to the magnetosphere to major geomagnetic disturbances and to the cross-polar cap potential [e.g., *Reiff et al.*, 1981; *Baker et al.*, 1984; *Burke et al.*, 1999; *Lu et al.*, 1998; *Freeman and Farrugia*, 1999]. This aspect of the work will bring out the extraordinary character of the May 1998 event during the rising phase of solar cycle 23. Through a study and modeling of major magnetospheric

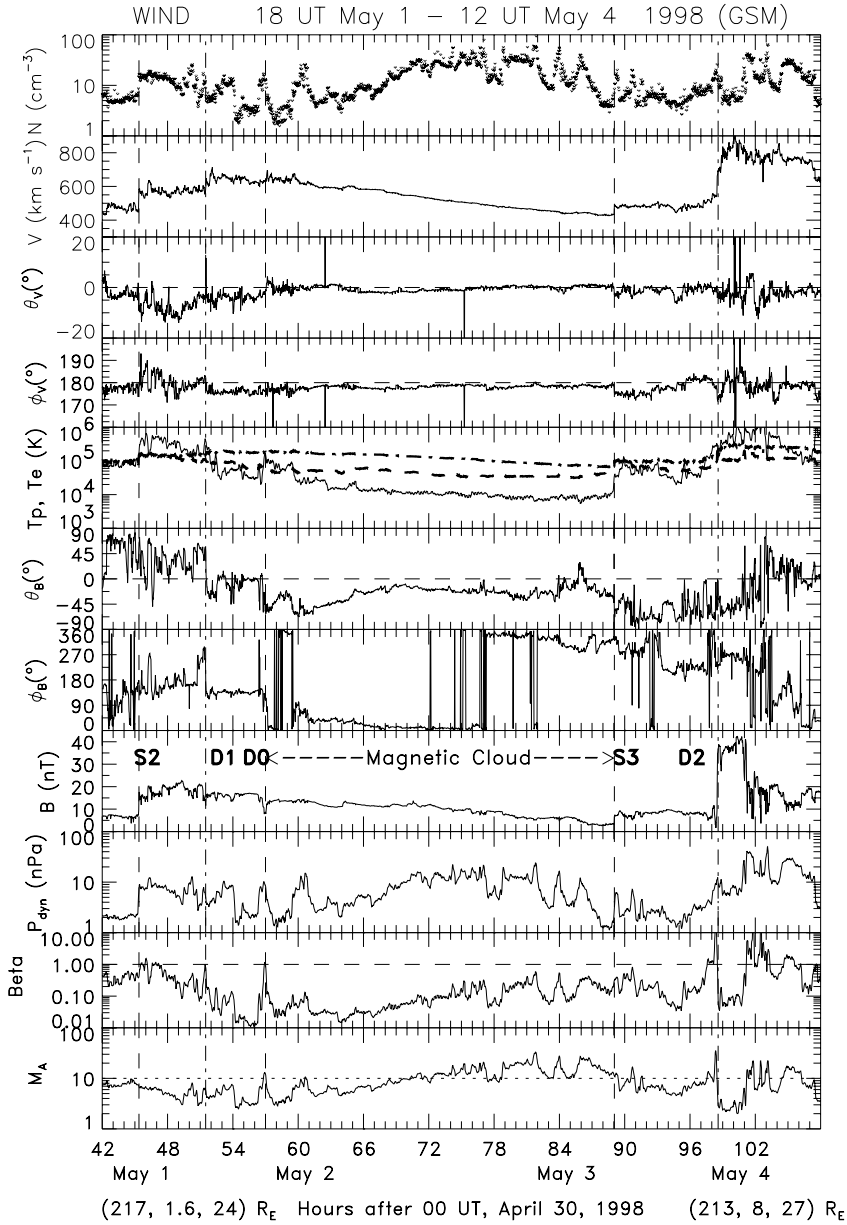

Figure 1. Particle and magnetic field measurements from Wind for the period 1800 UT, 1 May to 1200 UT, 4 May. From top to bottom: the proton density, bulk speed, latitude, and azimuthal flow angles, proton (solid trace) and electron (dashed trace) temperatures, the GSM latitude and azimuthal direction of the magnetic field, the total field, the solar wind dynamic pressure, the proton beta, and the Alfven Mach number. The dot-dash curve in panel 5 gives the expected temperature for normal solar wind expansion, after *Lopez* [1987].

current systems, the second paper will discuss how this unprecedented power and energy input affected the magnetosphere.

2. Observations

2.1. Wind: Magnetic Field and Plasma

[8] Interplanetary magnetic field and plasma observations from the Wind spacecraft for the period 1800 UT, 1 May 1 1200 UT, 4 May are shown in Figure 1, which displays from top to bottom, the proton density, bulk speed, the GSM latitude and longitude of the flow vector (0° longitude is sunward and 90° is east), the proton (solid trace) and electron (dashed trace) temperatures, the latitude and longitude of the magnetic field vector (0° longitude is sunward and 90° is east), the total field, the dynamic pressure, the proton plasma beta (ratio of plasma to magnetic pressures) and the Alfven Mach number. (The horizontal axis is marked in hours from 0000 UT, 30 April because we shall have occasion to study data on 30 April below.) The dotted-dashed trace in the fifth panel gives the proton temperature of the solar wind expected for normal solar wind expansion, following the statistical studies of *Lopez* [1987]. Temperatures significantly lower than this are considered to be a

reliable indicator of ejecta material in space [*Gosling et al.*, 1973; *Richardson and Cane*, 1995] (see also review by *Gosling* [1990, and references therein]). The spacecraft was located at (217, 1.6, 24) R_E and (213, 8, 27) R_E (GSE coordinates) at the start and end of the period shown, respectively. With such small displacements from the Earth-Sun line Wind was ideally placed to monitor solar wind conditions affecting Earth.

[9] Various key times have been marked by vertical guidelines. In the interval between the innermost vertical guidelines the fluctuation level in the magnetic field is lower than in the surrounding medium, the magnetic field strength is generally higher than typical values at 1 AU (of the order of 5 nT), the magnetic field vector executes a large rotation, the proton temperature is about a factor of 5 below that expected from solar wind expansion, and the proton β is $\ll 1$. These criteria identify interplanetary magnetic clouds [*Burlaga et al.*, 1981, 1990]. This interval was also identified as such by *Skoug et al.* [1999]. (With respect to the location of the cloud front boundary, labeled D0, ours is 3 hours earlier, a determination justified farther below.) That the time of the front boundary of the magnetic cloud (D0) in Figure 1 indeed marks a crossing of a topological interface will be supported by energetic and compositional data discussed below. The declining bulk speed profile indicates that the magnetic cloud is radially expanding [*Klein and Burlaga*, 1982]. On 3 May up to the time marked S3, the proton and electron temperatures are very low ($\sim 10^4$ and $\sim 3.5 \times 10^4$ K, respectively) and decreasing. Simultaneously densities are generally high, with large values in excess of 50 cm^{-3} reached on occasion.

[10] On the basis of the elevated He^{++}/H^+ relative concentration ratios (average ~8%) and the presence of heat flux electrons counterstreaming along the field, a reliable signature of ejecta material in space [*Gosling et al.*, 1987; *Gosling*, 1990], *Skoug et al.* [1999] suggest the presence of a ICME extending from D1 at 51.5 hours to D2 at 98.6 hours in Figure 1. Indeed, comparison of proton temperatures with those expected for normal solar wind expansion show generally lower temperatures in this interval. We shall adhere to this identification and concentrate in the rest of this section on (1) the nature of D1 and D2 and (2) the behavior of solar wind electrons on 2–4 May 1998.

[11] We next searched for the solar sources of this ejection. The most likely candidate would seem to be the halo CME visible in LASCO/C1 from ~1620 UT, 29 April, with a speed of 960 km s^{-1} in the plane of the sky. This CME is associated with the M6.8 flare in AR8210 from 1606 to 1659 UT, peaking at 0637 UT.

2.1.1. Shocks

[12] Two interplanetary shocks passed Wind during the time interval shown in Figure 1, one at 2121 UT, 1 May (labeled S2) and one at 1657 UT, 3 May (S3). (A third shock observed at ~0840 UT, 30 April (S1) will be discussed below in connection with energetic particles.) We used the coplanarity theorem on the 3-s resolution magnetic field to determine the shock normals and the shock speeds [*Abraham-Shrauner and Yun*, 1976], taking average values over 5 min on either side of the shocks. We obtain the following results: $\mathbf{n_2}$ = (0.99, −0.12, −0.02) and V_2 = −631 km s^{-1} (S2); $\mathbf{n_3}$ = (−0.90, 0.38, −0.20) and V_3 = 492 km s^{-1} (S3). The shock speed V_2 is comparable to that of the leading edge of the ICME, consistent with this shock being driven by the ejecta. In contrast, V_3 is substantially higher than the ambient speed, indicating that S3 is overtaking the ejecta.

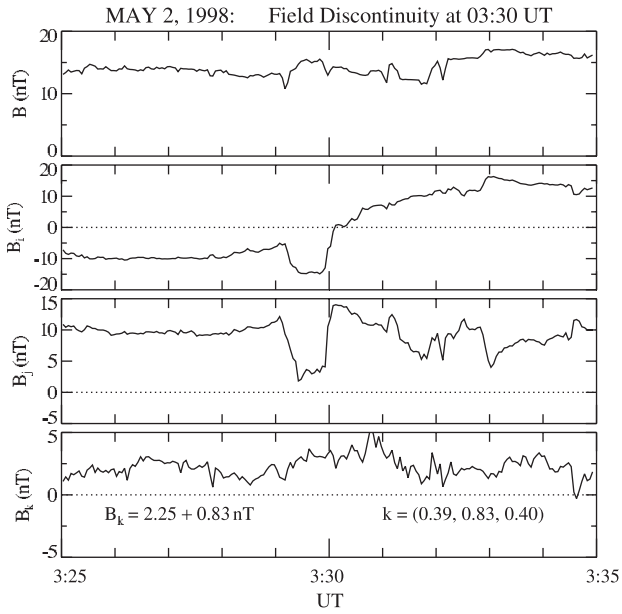

Figure 2. Magnetic field data at 3-s resolution plotted in principal axes coordinates (i, j, k) for the discontinuity D1 centered at 0330 UT, 2 May.

2.1.2. Directional discontinuities

[13] We next discuss the field directional discontinuites D1 and D2. At D1 the interplanetary magnetic field (IMF) rotates abruptly east and south (Figure 1, panels 6 and 7), and there are associated changes in the flow direction and speed (see also below). Minimum variance analysis [*Sonnerup and Cahill*, 1967] of the 3-s resolution MFI data suggests that this discontinuity is rotational. Figure 2 displays the data for a 10-min interval centered around this discontinuity at 0330 UT, 2 May in the principal axes system (i, j, k). With an intermediate to minimum eigenvalue ratio of 9.8, these results should be reliable [*Sonnerup and Cahill*, 1967; *Lepping and Behannon*, 1980], and a central nesting of the interval shown in Figure 2 gave essentially the same results as quoted above. The field has a clear nonzero component in the direction perpendicular to the plane of the discontinuity (**k**) given by **k** = (0.39, 0.83, 0.40) of B_k = 2.25 ± 0.83 nT.

[14] Figure 3 displays plasma and magnetic field parameters for 0300–0400 UT, 2 May centered on this discontinuity: the proton density, pairwise components of the flow and field in principal axes coordinates, the proton bulk speed and temperature, the total field, the proton beta, the sum of the plasma and magnetic prerssure, p_t, and the Alfven speed. There are plasma features consistent with the rotational character of D1: (1) a flow speed enhancement of the same order of magnitude as the local Alfven speed (~100 km s^{-1}; eight and last panels); (2) generally satisfactory correlated rotations of the field and flow components (panels 2 to 7); and (3) a finite component of flow (v_k) across the discontinuity. More quantitatively, taking as reference point the short interval just before the disconti-

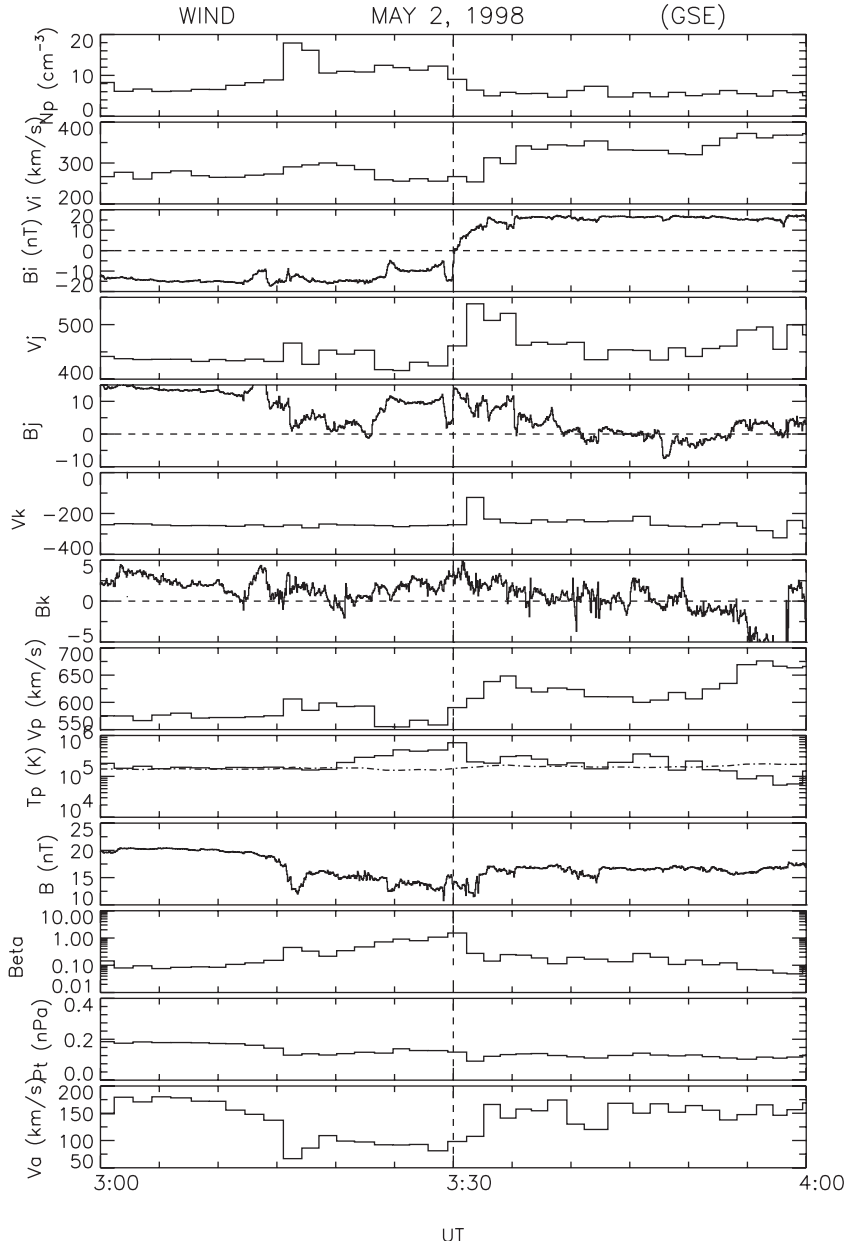

Figure 3. Plasma and field parameters for 0300–0400 UT, 2 May plotted in (i, j, k) coordinates: (top to bottom) density, (pairwise) flow and field components, the proton bulk speed, and temperature, the total field, the proton beta, the sum of the proton thermal, and field pressures, p_t, and the Alfven speed.

nuity (0329 UT) and analyzing the interval 0330–0335 UT by interpolating the 3s-resolution field data with the 90-s plasma data (four points), we find that (1) the angles between $\Delta\mathbf{V}$ and $\Delta\mathbf{B}$ are 55, 86, 61, and 60°; (2) average $\Delta V_p/V_A$, where V_A is the Alfven velocity is 0.8; (3) average $\Delta B/B$ = 1.3. Thus the evidence for the rotational character of D2 from the plasma data is fair. The discontinuity D1 is propagating antisunward because the field and flow components are positively correlated and the IMF points toward the Sun. Just ahead of, and at, D1 localized heating is evident (panel 9), which occurs when the field is depressed, with quantity p_t remaining fairly constant (pressure-balanced structure). This is a good example of a magnetic hole. The conversion of magnetic field energy into particle heating may represent a slow shock feature. The combination of a rotational discontinuity and a magnetic hole could further indicate the presence of a reconnection layer at the leading edge of the ejecta (see also Discussion). The low resolution of the plasma data precludes, however, a more quantitative assessment in this case.

[15] The discontinuity D2 forms the leading edge of the high-speed stream at which the magnetic field strength is very elevated. For clarity, the period 0000–1000 UT, 4 May is shown in Figure 4, in the same format as Figure 1. A search for recurrence at the solar rotation period through 5 months of solar wind streams indicated that the May 4 high-speed stream was transient, i.e., noncorotating. The discontinuity D2 is not a shock (see also *Skoug et al.* [1999]) as

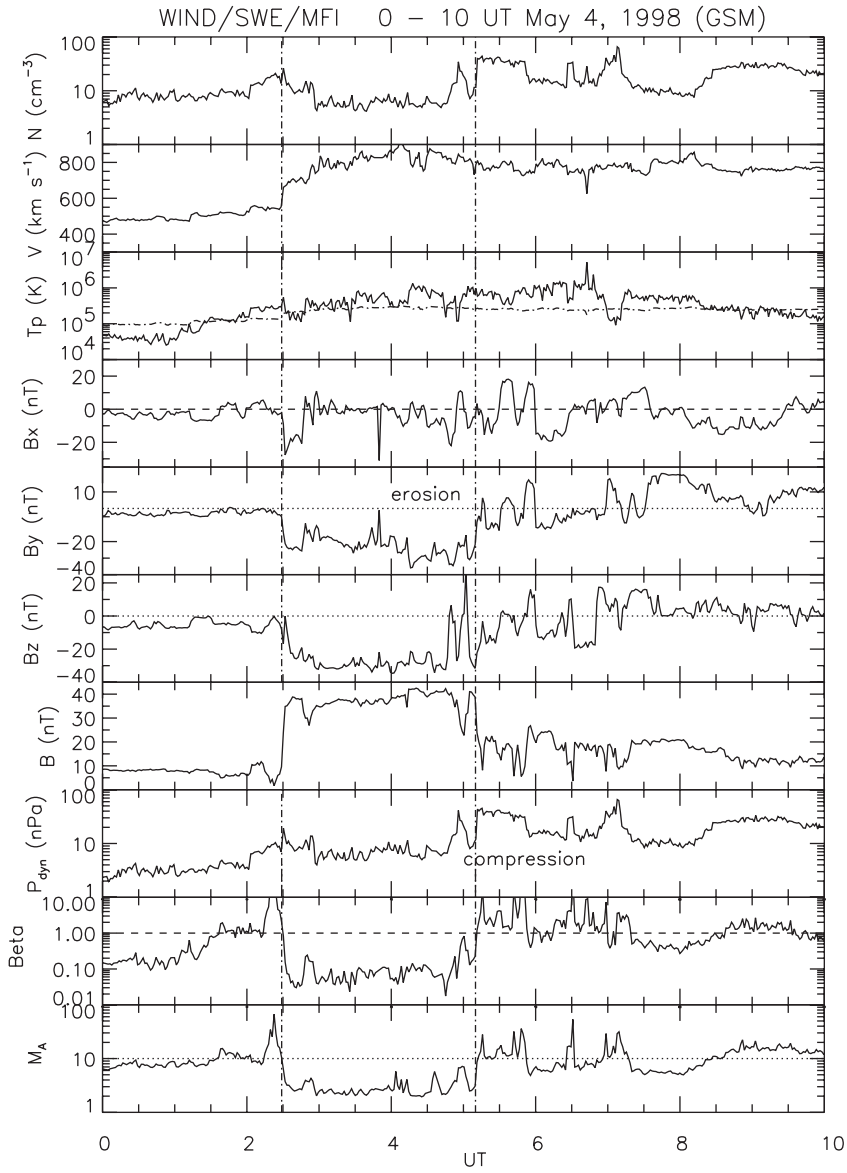

Figure 4. Plasma and field parameters for the period 0000–1000 UT, 4 May: proton density, bulk speed and temperature, GSM components of the magnetic field, total field, dynamic pressure, proton plasma beta and Alfven Mach number. The labels ''erosion'' and ''compression'' designate two periods of large, negative IMF B_z and high dynamic pressure, respectively, which occur almost sequentially.

can be seen from the very small and gradual changes in proton density and temperature. Minimum variance analysis over the interval 0200–0300 gave a very accurately defined normal (ratio of intermediate to minimum eigenvalues of 64) of **k** = (0.53, −0.52, 0.66). The normal component of the magnetic field $B_k = -0.5 \pm 1.2$ nT, i.e., consistent with zero. There is, however, a large pressure imbalance across D2, mainly due to the magnetic pressure, excluding the possibility that D2 is a tangential discontinuity. $B_k = 0$ implies that the high-speed, strong-field region behind D2 is magnetically isolated from the preceding magnetic cloud and may be acting as a piston driving shock S3. A minimum variance analysis of the magnetic field data from 0200 to 0510 UT gave a good normal determination (ratio of intermediate to minimum eigenvalues of 3.5), which is inclined by ∼14° to the normal **k**. Thus the field fluctuations in the high-speed stream on 4 May are mainly confined to a plane approximately parallel to its front boundary D2. The field components in (i, j, k) coordinates determined from minimum variance analysis over the interval 0200–0300 UT are shown in Figure 5.

[16] For ∼3 hours behind D2 (∼0230 to ∼0510 UT, 4 May), Wind measures very extreme values of the interplanetary parameters (Figure 4): a very strong field (B ∼ 40 nT) and strongly southward ($B_z \sim -35$ nT) and westward pointing ($B_y \sim -30$ nT) field, high-speed (800–900 km s^{-1}), low proton β (∼0.06) and low Alfven Mach number, M_A (∼2.5). These values account for the strong interaction of this stream with Earth's magnetosphere and motivates the considerations of power in section 3. Solar wind–magnetosphere ''coupling parameters'' depend directly on interplanetary B_z and the bulk speed [e.g., *Baker et al.*, 1984, and

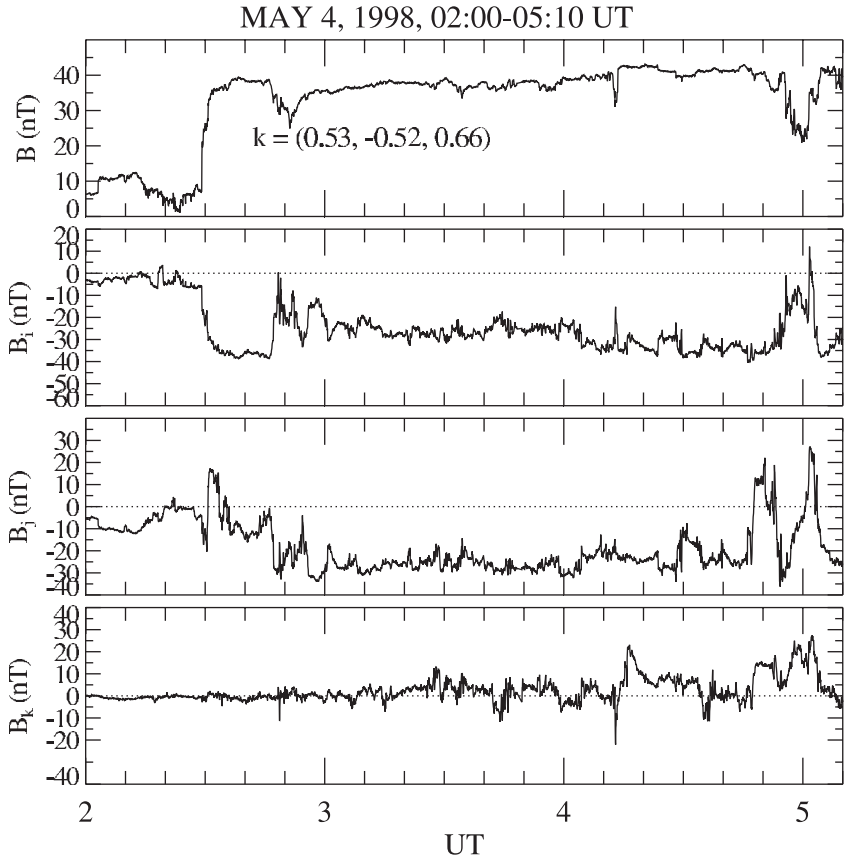

Figure 5. Wind/MFI magnetic field data for the high-speed stream on 4 May 1998 (erosion phase) plotted in principal axes coordinates in the same format as Figure 2. For further details, see text.

references therein]. Very low solar wind beta values are expected to lead to low beta values in the magnetosheath, which are thought to favor strong reconnection at the low-latitude magnetopause [*Paschmann et al.*, 1986]. Low values of M_A imply a strong control of magnetosheath flow by the IMF [*Farrugia et al.*, 1995]. The period 0230–0510 UT, 4 May may be termed the "erosion" phase, since wholesale erosion of the dayside magnetosphere may be anticipated (and was observed (J.-H. Shue, private communication, 2000; C. Farrugia et al., manuscript in preparation, 2002). It is followed with only a slight overlap by a long period of high dynamic pressure (10–40 nPa; labeled compression phase). The almost sequential occurrence of these two phases helps to separate their respective geomagnetic effects (C. Farrugia et al., manuscript in preparation, 2002).

2.1.3. Solar wind electrons

[17] The behavior of solar wind electrons of core and halo energies as obtained from the SWE instrument on Wind is shown in Figures 6a–6c. In the energy spectra of Figure 6a, intensities (counts), averaged over spin phase, are displayed over a logarithmic scale according to the color bar on the right. Shown is the period 1–4 May 1998. The energy range of the SWE vector electron and ion spectrometer (VEIS) shown here extends from 13 to 973 eV. Enhanced fluxes are evident in the interval between shock S1 (30 April) and S2 (1 May), and at shock S3. Intensities maximize at the shocks S2 and S3 themselves. An even stronger enhancement starts at interface D2 on 4 May and continues up to ~1200 UT, 4 May. In the interval 0200–0800 UT, 4 May it appears as a multistage enhancement. Remarkably, on 2 May 1998, after the enhancement at shock S2, the halo population is considerably weakened, except for a recovery during ~1700–1900 UT. On 3 May from 0000 UT up to the shock S3, the halo population is further weakened and, possibly as a consequence, the low-energy core of the electron velocity distribution is seen to become very tenuous in the measured energy range, indicating that the core electrons are primarily at energies lower than 13 eV. The very weak halo on 3 May may indicate that the field lines of the magnetic cloud were severed from the Sun. However, dropout of the halo is a necessary, but not sufficient, indicator of magnetic field line disconnection [*Lin and Kahler*, 1992]. The weak halo may, however, also result from either (1) the plasma being too cold to have significant count rates above the SWE/VEIS instrumental threshold, or (2) scattering by enhanced Coulomb collisions. We examine the latter possibility next.

[18] We consider the electron-electron Coulomb collision rate (ν) for a 90° deflection for two solar wind states: (1) One with parameters typical of the (borderline) fast solar wind, taken from the review by *Isenberg* [1991], and (2) one with the parameters on 3 May. We have for (i) $n_{e1} = n_{p1} = 4\ \mathrm{cm}^{-3}$ and $T_{e1} = 1.0 \times 10^5$ K. For state 2 we take general

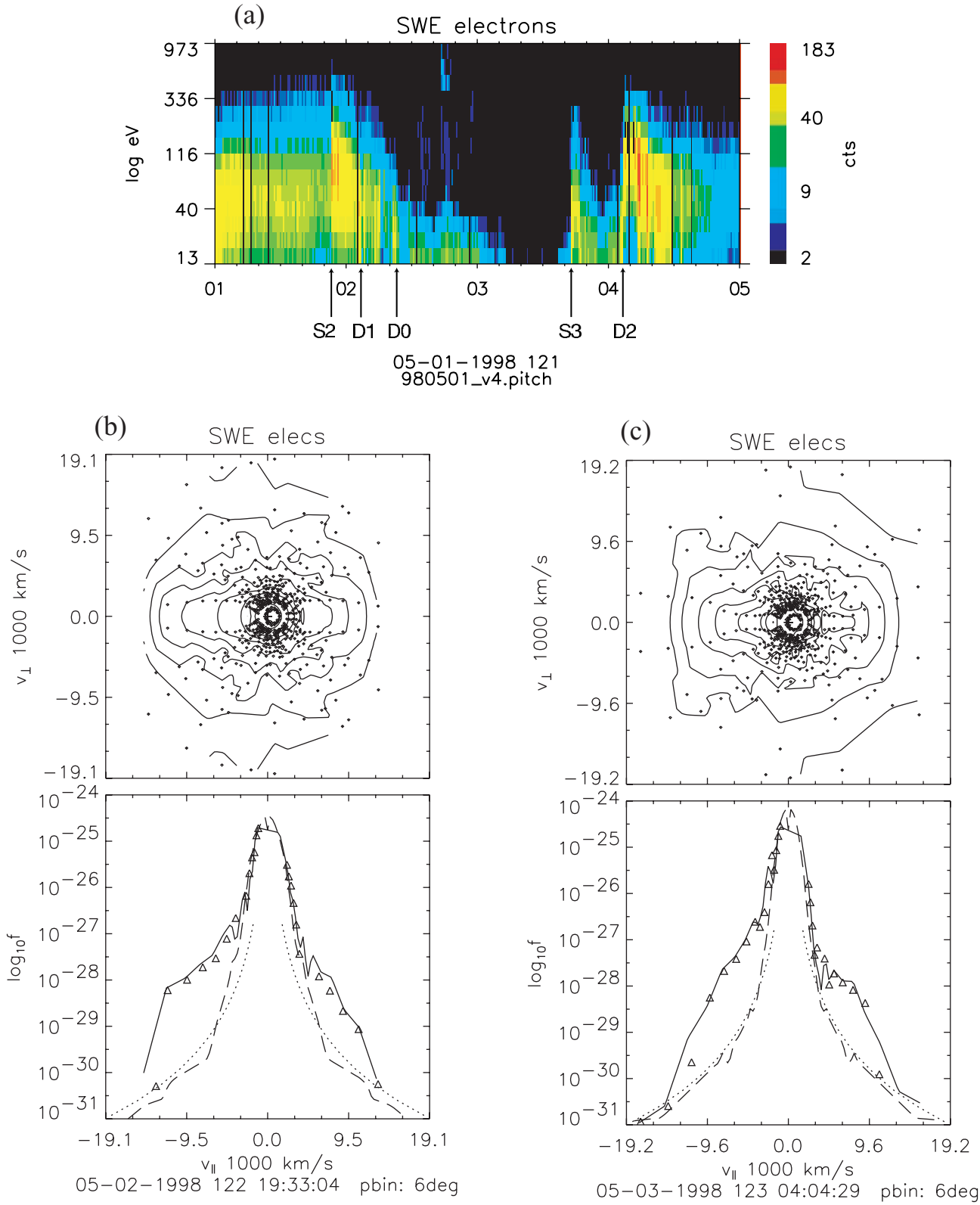

Figure 6. (a) Wind/SWE VEIS electron spectrum for 1–4 May 1998. Note (1) the enhancements at the shocks and at the TD on 4 May; (2) The very tenuous halo and low-energy core of the electron distribution on 3 May in the measured energy range (13–973 eV), the latter indicating that electrons are primarily below 13 eV. Two examples of pronounced electron bidirectional streaming from Wind/SWE, on (b) 2 May and (c) 3 May.

values for 3 May: $n_{e2} = n_{e2} = 40$ cm^{-3} and $T_{e2} \approx 3.5 \times 10^4$ K (Figure 1). The Coulomb collision rates (ν_1 and ν_2) are then related by

$$\nu_2 = \nu_1 (n_{e2}/n_{e1})(T_{e1}/T_{e2})^{3/2}$$

i.e., the collision rate for a 90° deflection has increased by a factor of ~48. The mean free paths (l_1, l_2) are $(kTe/me)^{1/2}/\nu$, and we have $l_2 \approx 0.01 l_1$. Thus, while Coulomb collisions are negligible for electrons with typical solar wind T_e and n_e ($l_1 \approx 0.41$ AU, after inserting numerical constants), they should be important in the high-density–low-temperature situation on 3 May ($l_2 \approx 0.004$ AU). This supports the Coulomb collision mechanism (2).

[19] Bidirectional streaming of heat flux electrons, extending for most of 2 and 3 May has been noted by *Skoug et al.* [1999], briefly interrupted during the intervals 2200 UT; 2 May to 0100 UT, 3 May; and 1500–1900 UT, 3 May [*Skoug et al.*, 1999, Figure 1]. Two examples of strong bidirectional flows from Wind/SWE are shown in Figures 6b and 6c referring, respectively, to 1933:04 UT, 2 May, and 0404:29 UT, 3 May. The top panel is the velocity distribution plotted in velocity coordinates parallel (horizontal) and perpendicular (vertical) to the magnetic field. The underlying points are the velocity coordinates of the measurements. The bottom panel shows the parallel cut through the distribution (solid curve), the perpendicular cut (dashed curve), and the one-count level (dotted curve). The triangular symbols are the measurements closest to the magnetic field. The distribution function at energies below the lowest measured energy of 13 eV is represented by a fitted Gaussian based on the measurements between energies 13 and 30 eV in all directions during one spacecraft rotation. The density and flow speed derived from the gaussian core are in qualitative agreement with the ion density and flow speed for the distribution shown here.

[20] *Gloeckler et al.* [1999] and *Skoug et al.* [1999] note a distinguishing feature of this ICME in the form of a prolonged interval of anomalous composition (high) He^+/He^{++} values) extending continuously throughout 3 May up to ~0100 UT, 4 May. They also note the very low proton temperatures during most of the magnetic cloud interval up to S3 (~10^4 K, see Figure 1). These observations were attributed to the presence of prominence material. We further note that this prominence material was associated with a very weak solar wind electron halo.

2.2. Energetic Particles

[21] Observations of solar energetic particles, composition, and charge states help to confirm and clarify the nature of the boundaries/discontinuities identified above and reveal further features that relate the observations at 1 AU with events on the Sun. Data from various instruments on both ACE and Wind are shown, as detailed in the introduction. ACE was at an average position (228, −32, −16) R_E (GSE coordinates); that is, it was on the opposite side of the Sun-Earth line and separated from Wind by only ~14 R_E in the X- and ~34 R_E in the Y directions. Thus observations of shocks at the two spacecraft are expected to be approximately simultaneous. As regards composition, we shall focus on He and Fe. Because of its wide range of available charge states, iron is a particularly useful diagnostic for the origin of solar energetic particles (SEPs), whether produced in impulsive (flares) or in gradual (shocks associated with ejecta) events. The charge states can be altered by the temperature in the source region or by electron stripping.

[22] Proton observations from EPACT, and electrons measured by EPAM for the interval 30 April to 4 May 1998, are shown in Figure 7. The figure plots from top to bottom differential fluxes of protons in the energy range 28–72 MeV/nucleon from the Low Energy Matrix Telescope (LEMT) on EPACT, proton intensities from the Suprathermal Energetic Particles (EPACT/STEP) instrument in three channels, namely, H3 (E = 0.16 – 0.23 MeV; dark trace), H6 (E = 0.46 – 0.65 MeV; red trace), and H10 (E = 1.74–2.51 MeV), solar energetic electrons from the deflected electron spectrometer DE30 on EPAM in two energy passbands corresponding to 0.038–0.053 MeV (de1) and 0.175–0.315 MeV (de4); and the total magnetic field; the bulk flow speed; and the B_z component from Wind for reference. The DE30 telescope is oriented at 30° to the spin axis of the spacecraft, which points within ±30° of the Sun direction. EPACT data in the first panel are at ~90-s time resolution shown as ~30-min averages; EPACT/STEP proton data are at ~10-min resolution; EPAM fluxes are 1-hour averages, plotted at the half hour. Vertical guidelines are drawn as in Figure 1, and we have added a guideline to show the arrival time of the shock S1, as observed by Wind on 30 April.

2.2.1. Magnetic connection to flare sites

[23] After a general rise between S1 and S2, followed by a smooth decrease after S2, EPACT fluxes of high-energy protons show two major features of interest. First, they record a small but clear depression at ~0900 UT, 2 May (hour 57; labeled D0, as in Figure 1), i.e., at what we have identified as the leading edge of the magnetic cloud [see also *Skoug et al.*, 1999]. Such depressions, which result from the inability of protons at these energies to diffuse effectively across magnetic field lines [*Cane et al.*, 1995], are considered to be a robust signature of the entry of the spacecraft into the closed magnetic field line region of ejecta [*Richardson*, 1997, and references therein], supporting our previous identification of a topological boundary at this time. Second, an enhancement by over 2 orders of magnitude is observed at 1410 UT, 2 May (hour 62.2), which is even more pronounced in the lower (19–28 MeV) energy channel (not shown). This is a prompt onset of solar energetic particles from a solar flare, identified below, and indicates that ejecta magnetic field lines at this time are still connected to the flare site and have guided the particles injected at the flare to the spacecraft [*Kahler and Reames*, 1990; *Richardson et al.*, 1991; *Farrugia et al.*, 1993a, 1993b].

[24] This prompt onset is also registered as a sharp increase of proton fluxes in all three lower-energy channels of STEP (panel 2), but the flux increases at these lower energies are delayed with respect to the high-energy protons by ~4–5 hours. (We note that the solar particle event was accompanied by high intensities, which resulted in a reduction of the proton efficiency of the STEP instrument. We have compensated for this effect by scaling the measured proton intensities from 1400 UT on day 122 through day 126 according to the average H/He ratio measured by STEP at appropriate energies from 1200 UT on day 120 through

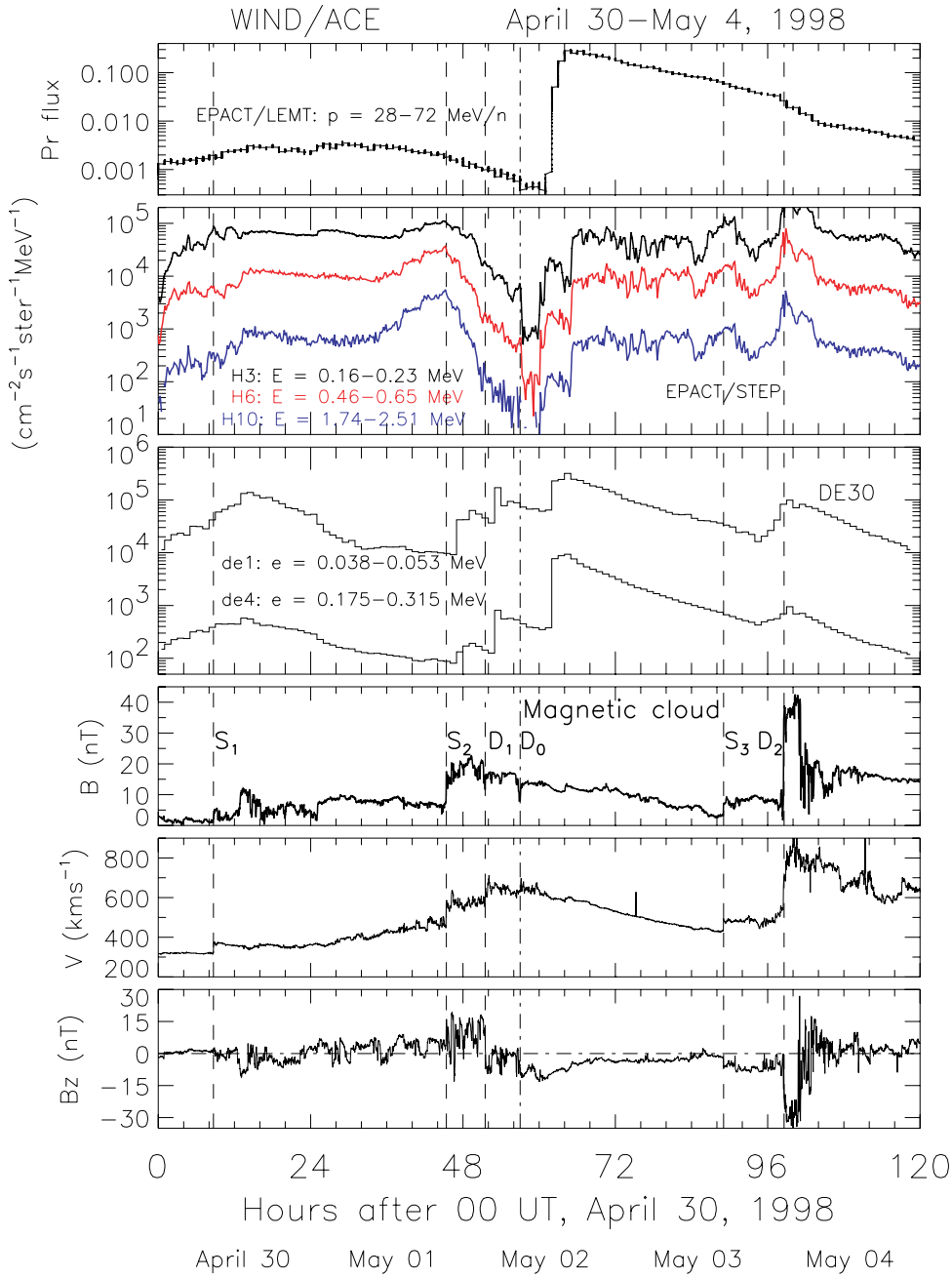

Figure 7. (top to bottom) Differential fluxes of protons (E = 28–72 MeV/nucleon) from EPACT/LEMT; proton intensities from EPACT/STEP (color-coded as indicated), energetic electrons from EPAM/DE30 in two energy passbands; the total magnetic field, proton bulk speed, and B_z component of the field from Wind. Key times identified earlier have been indicated by vertical guidelines.

1200 UT on day 121.) Electrons are injected as well (panel 3). Since at these energies electrons are highly relativistic, they are expected to fill the flux tube within a few minutes of injection. Thus the electron onset is practically coincident with the EPACT/LEMT high-energy proton onset.

[25] A likely candidate for the flare responsible for this EPACT proton injection observed inside the magnetic cloud starting at ~1410 UT, 2 May is the X1.1 event from 1331 to 1351 UT, 2 May with peak at 1342 UT. (All flare times quoted in this paper are from the NOAA/GOES Web site, see acknowledgements.) This allows a ~30 min delay for the EPACT protons (panel 1) and the DE30 electrons to arrive at 1 AU, a reasonable estimate. The flare caused a large particle event at SOHO and probably originated in AR 8210 located at S15W15. This flare site would not normally have good connection to Earth along Parker spiral magnetic field lines, so that the fact that Wind nevertheless observed flare particles implies that the spacecraft is on magnetic field lines connected directly to the flare. The only other GOES event within a reasonable time frame was a B6.5

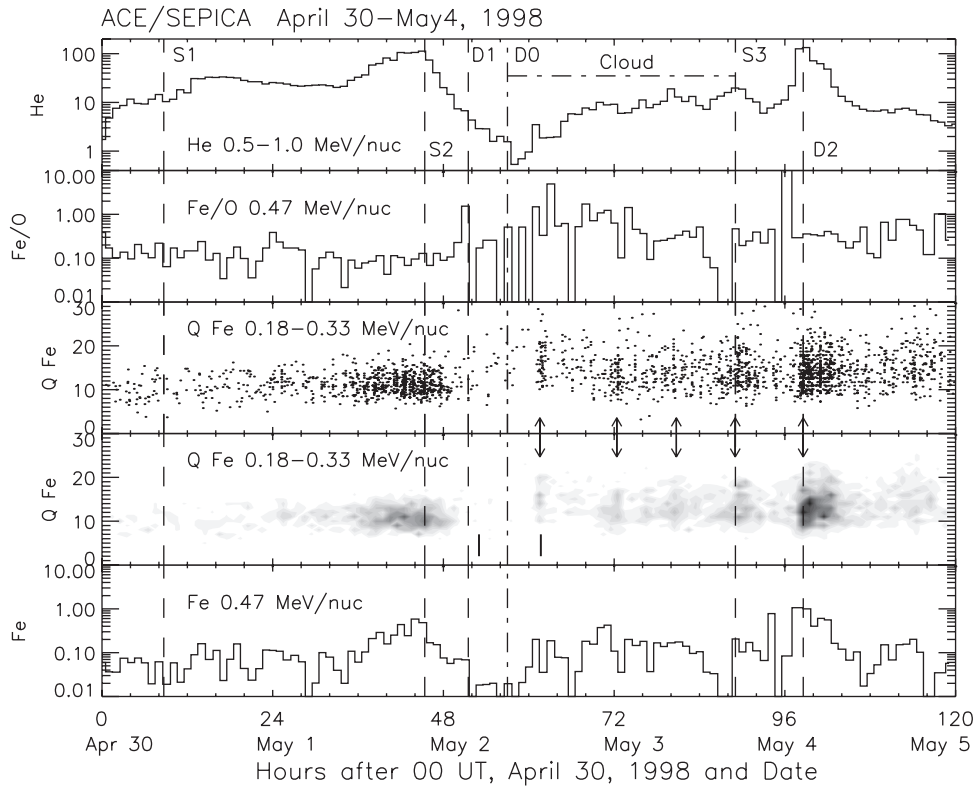

Figure 8. ACE/SEPICA measurements on He and Fe. (top to bottom) He flux at 0.5–1.0 MeV/nucleon; the Fe/O ratio at 0.47 MeV/nucleon; iron charge states at 0.18–0.33 MeV/nucleon (in two formats); and Fe flux at 0.47 MeV/nucleon. Vertical guidelines are drawn at the same times as in Figure 8.

event during 1314–1319 UT, 2 May with peak at 1317 UT. However, besides being far too weak, this flare would be inconsistent with the arrival of the highest energy protons.

[26] Actually, looking at panel 2, Figure 7, there is another sharp increase in proton fluxes at ~1200 UT, 2 May (hour 60), seen most clearly in the energy channels H3 and H6, i.e., ~5–6 hours prior to the one just described. Since both injections refer to the protons of the same energy, this earlier proton flux increase suggests an injection from an earlier flare. The abrupt variations in STEP proton fluxes thus imply magnetic connection to at least two flare sites at two different times.

[27] The temporal variation of the STEP proton intensities show further features of interest. Between shock S1 and S2 the intensities are high. Localized intensity spikes at S2 and S3 are evident. Further, at S2 the highest-energy protons (H10; blue trace) undergo the largest enhancement, whereas at S3 approximately the same fractional increase is recorded in all three energy channels. A strong decrease in STEP proton intensities occurs during hours 84–87 similar to, but weaker than, the depression at the front boundary of the magnetic cloud. This depression may indicate further structure within the magnetic cloud. Finally, we note the large local enhancement lasting ~4 hours in STEP proton intensities at D2 on 4 May, which is even more pronounced than that at the shocks. Evidently, at this resolution it consists of a twin-peaked enhancement. We recall that behind D2 a very strong magnetic field was observed. Fluxes continue at high levels through 4 May.

[28] EPAM/DE30 records an injection of energetic electrons at ~0430 UT, 2 May (hour 52.5) shortly after the rotational discontinuity D1 ahead of the magnetic cloud observed by Wind/MFI, noted in the previous section. Keeping in mind the 1-hour resolution of the electron data, the timing of the electron flux increase makes it fairly consistent with an injection from a flare at 0329 UT, peaking at 0334 UT, 2 May. In summary, in the 1–4 May 1998 configuration, there are SEPs typical of both gradual (ICME-associated shocks) and impulsive (flare-associated) events. The latter arrive at 1 AU from different flares.

2.2.2. Composition

[29] We now discuss composition. Ionic charge states and elemental composition show a variety of energetic particle populations during 30 April to 4 May 1998. Figure 8 shows from top to bottom measurements of He at 0.5–1.0 Mev/nucleon; the Fe/O ratio at 0.47 MeV/nucleon, at approximately the same energy as the charge state measurements; charge states for individual iron ions at 0.18–0.33 MeV/nucleon (grayscale; panels 3 and 4); and finally, the Fe flux at 0.47 MeV/nucleon. The data are at 1-hour resolution. Vertical lines have been drawn at the same times as in Figure 7.

[30] The He energy is similar to the energy of the STEP protons from energy channel H6 (Figure 7) and, indeed, the temporal variation of both species, measured by different instruments, agree remarkably well in many respects. As observed in the protons, the He intensity was high between

shocks S1 and S2 (first two vertical guidelines), peaking near S2. The He flux decreased after S2 and then decayed abruptly to a minimum at 0900 UT, 2 May (D0; hour 57) at the magnetic cloud front boundary. At ~1200 and ~1700 UT, 2 May, two He flux increases are observed. These occur at the same times that two enhancements in STEP H6 fluxes separated by ~5 hours were observed, as noted above. Thus these He flux enhancements represent the time-delayed arrivals of He injected at the same two flares. We have identified the later flare with the GOES event peaking at 1342 UT. The earlier flare might be the one peaking at 1020 UT, but on the GOES Web site its position is not specified.

[31] Inside the cloud, He has a fluctuating flux profile, with three principal peaks at 2100 UT, 2 May; 0800 UT, 3 May; and 1700 UT, 3 May (hours 69, 80, and 89, respectively); the last of these coinciding with the shock S3 (fifth vertical guideline in Figure 8). We may note analogous behavior in the iron charge states (panels 3 and 4) during cloud and ICME passage: a striated appearance is evident here, with individual intensifications marked by arrows in panel 4 (see below). The middle three arrows correspond to times noted above when He is enhanced within the cloud. Later, on 4 May a strong He enhancement occurred at the front edge of the high-speed stream, from 0100 to 0700 UT, 4 May. The iron, discussed below, shows, too, evidence of separate enhancements during this period.

[32] The solar energetic particle (SEP) iron population during 30 April had a mean charge state of 10.2, which is similar to what is found in ions of typical solar wind energies (~1 keV/Q) with the ACE/SWICS instrument [*Gloeckler et al.*, 1999]. This was followed by an intensification of iron at the beginning of 1 May, extending until 0200–0300 UT, 2 May, i.e., within the data resolution, ending before the rotational discontinuity D1 at 0330 UT. The intensity maximizes at approximately the same time as the arrival of shock S2 at 2121 UT, 1 May (second vertical guideline). As also shown in the top panel of Figure 9, which displays a histogram of Fe charge states for 2000–2100 UT, 1 May, these iron ions had a mean charge state of 11.5, which is higher than that of the 30 April population, and ~1–2 charge states higher than in the solar wind population at the same time [*Klecker et al.*, 2000]. The difference in SEP charge states with respect to the solar wind might result from differing properties of the shocks S1 and S2. The behavior of SEP iron at shock S2 has been discussed in detail in terms of rigidity-dependent acceleration from the solar wind population by *Klecker et al.* [2000]. That the SEPs observed near shock S2 may be accelerated locally by the shock is suggested both by the temporal association as well as by the approximate similarity of the SEP iron charge states to those of the solar wind, as discussed by *Klecker et al.* [2000]. At and in between shock S1 and S2 the Fe/O ratio at 0.47 MeV/nucleon (second panel) was at a low value of ~0.1, as is typical of SEPs accelerated in gradual, shock-associated events [*Reames*, 1999].

[33] Very little iron was observed between the 1 May SEP event and a subsequent injection just inside the cloud at ~1330 UT on 2 May (first double-headed arrow in panel 3, Figure 8). The iron injected just inside the cloud at the time had a mean charge state of 16+ (third panel) that was significantly higher than in the preceding period, and measured charge states inside the cloud extended from 10+ to 20+. The Fe/O ratio (panel 2) also increased which, together with high iron charge states, is consistent with an impulsive, flare-related source [*Luhn et al.*, 1987]. The iron injection was temporally consistent with a source in the already mentioned C class flare at S20W07 in AR8210, peaking at 0521 UT on 2 May (first heavy vertical bar in panel 4), allowing for ~7–8 hours for the iron to reach 1 AU along magnetic cloud field lines, which is a reasonable estimate. Note that this is an earlier flare than the one at 1342 UT (second heavy bar) which was responsible for the prompt onset of EPACT protons identified above. Arrival of energetic particles from at least two different flares in the same active region occurring at ~8.4-hour separation suggests that the magnetic cloud retained magnetic connection to this region and repeated flaring injected at least two successive energetic populations into the cloud. The locations of the identified flare sites from which energetic particles are reaching Wind and ACE (S20W07 and S15W15) imply that the cloud footprint has a linear dimension equal to at least the separation of these flare sites, i.e., ~0.16 R_s (solar radii), yielding a lower limit to the area (assumed circular) of the magnetic cloud footprint on the Sun of 0.02 R_s^2 (~10^{10} km^2). Using energetic particle observations at 1 AU we have reached a conclusion consistent with LASCO imagery about the location of the cloud's solar sources.

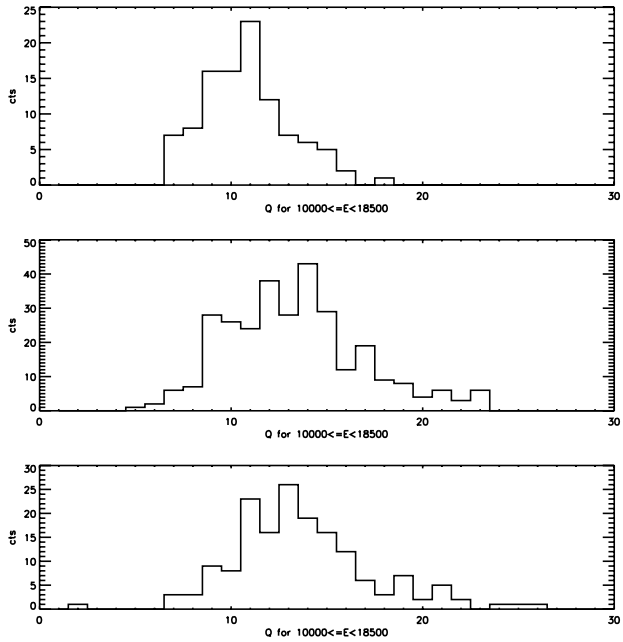

Figure 9. Histograms of SEP iron charge state each showing 1-hour intervals on 1 and 4 May as indicated. The top panel contains iron that was coincident with the passage of shock S2. The bottom panels show iron for the period of strong magnetic compression on 4 May. The bottom two iron samples have a higher mean charge and extend to higher charge states than the shock-associated sample at the top.

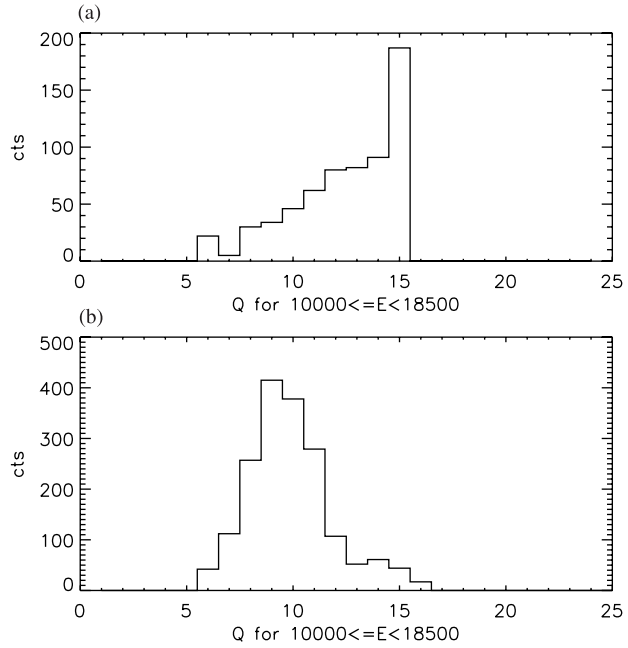

Figure 10. Solar wind Fe charge state histograms for (top) 0200–0600 UT, 4 May and for (bottom) 0200–1000 UT, 1 May. For further details, see text.

[34] For the rest of the cloud passage, the Fe/O was variable and a wide range of charge states was observed. From ~2000 UT, 2 May up to S3 during the time when (1) the halo electron population was tenuous and (2) SWE observed large and sporadic density enhancements, the iron shows remarkable features that may be summarized as follows.

1. A wide range of charge states are observed, from ~8 to ~20, i.e., corresponding, respectively, to what is normally seen in gradual events and what is seen in impulsive events.
2. The Fe/O ratio is highly variable.
3. There are localized enhancements in Fe flux, some of which coincide in time with the He enhancements mentioned earlier.
4. The charge states of the solar wind iron are also low; however, up to ~8 UT, the charge state distribution is bifurcated with simultaneous presence of $\geq$16+ iron and $\leq$8+ [*Popecki et al.*, 2000]. It is plausible that some of the SEP iron that we observe has been accelerated from the cold/hot solar wind population by the trailing shock S3 and has subsequently outrun the shock. The bursty enhancements in Fe flux, however, may be the result of further injections from the sun in a magnetically connected stucture.

[35] On 4 May, two more SEP enhancements occurred, coincident with the high magnetic field strength region. The first was at ~0200 UT, and the second was at ~0400 UT. The twin-humped time profile for iron can be seen in the bottom panel of Figure 8 in which the iron flux is plotted. From the middle and bottom panels of Figure 9, which show a charge state histogram of these two enhancements, it may be seen that the iron charge state distribution extends from ~10+ up to ~21+, with a peak near 13+. This was a somewhat higher charge state than that of the locally accelerated iron at shock S2 on 1 May. It extends to lower charge states in the first of the two enhancements (middle panel).

[36] Figure 10 shows a solar wind Fe charge state histogram for 4 May for 0200–0600 UT (top) and for 0200–1000 UT, 1 May (bottom). On 4 May a prominent contribution from charge state 16+ is clear. (The histogram has been cut off at 16+ for data analysis reasons.) In contrast, in the histogram for 1 May the relative contribution from Fe 16+ is much smaller. If the solar wind Fe is a seed population for shock acceleration, the difference in the solar wind Fe 16+ component between the 2 days may account for the differences in the two SEP Fe charge state distributions for the same days.

3. Considerations of Power

[37] A major feature of the interplanetary configuration on 1–4 May 1998, is the extraordinary amount of electromagnetic power it is potentially able to deliver to the magnetosphere. To investigate this aspect, we work in the formulation of *Perreault and Akasofu* [1978]. In their study of how the solar wind energy is dissipated inside the magnetosphere during stormtime periods, Perreault and Akasofu defined an "energy coupling" function ϵ as the fraction of the solar wind Poynting flux entering the magnetosphere. Parameter ϵ is defined by $\epsilon = \mu_0^{-1} V B^2 \sin^4(\theta/2)$, where V, B, θ are the solar wind bulk flow, IMF strength, and IMF clock angle (i.e., the polar angle in the GSM YZ plane), respectively, and μ_0 is the permittivity of free space. (We work in terms of energy flow (W m^{-2}).) From considerations of reconnection at the magnetopause, *Kan and Lee* [1979] extended *Sonnerup*'s [1974] pioneering study of the largest merging rate at the magnetopause and showed that ϵ is proportional to the power delivered by the solar wind to the magnetosphere.

[38] Figure 11 shows by the solid trace the time variation of this parameter over the 4-day period 1–4 May. The dashed trace gives its integral over time (in J m^{-2}) according to the scale on the right. Vertical lines have been drawn at the same key times as in Figure 1. Some powering of the magnetosphere occurs in the sheath region behind the shock S2, which increases after the field turns south at the rotational discontinuity D1. The steadily less negative B_z inside the magnetic cloud (Figure 1) leads similarly to a slowly decreasing power over ~1.5 days. The power increases somewhat behind shock S3 where B_z turns more negative (Figure 1). At the arrival of the leading front of the 4 May high-speed stream and in the ~3 succeeding hours of the "erosion phase" (Figures 1 and 4), the power rises sharply to a steady and high value (~0.75 mW m^{-2}). For the rest of 4 May the power is enhanced in a sporadic fashion. As the dashed trace shows, the energy input over just 3 hours during the high-speed burst behind D2 on 4 May is comparable to that accumulated during ejecta passage including the cloud sheath in the preceding 3 days, which is ~6 J m^{-2}.

[39] To put the above into a broader context, we compared the energy input on 4 May with eight other events (including 1–3 May 1998) spread over three solar cycles, labeled A–H in Figure 12, which shows the distribution of

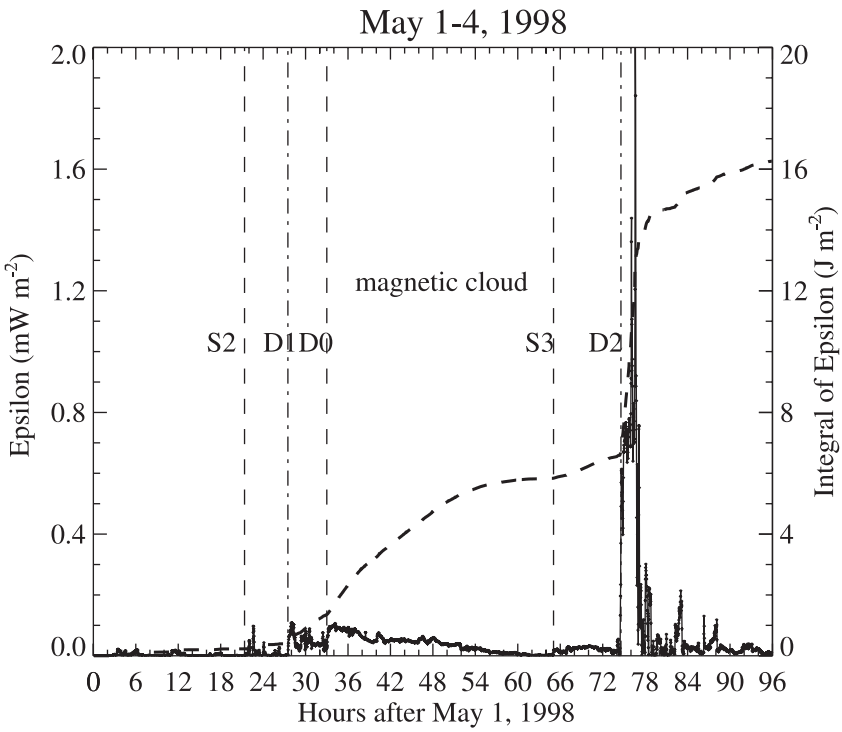

Figure 11. Variation of the electromagnetic power input to the magnetosphere during 1–4 May 1998, based on the formulation of *Perreault and Akasofu* [1978] (left scale; dark trace); and the resulting energy deposition (right scale, dashed trace).

these events with respect to solar cycle. It displays the monthly sunspot numbers from January 1970 to December 2000. A solid line joins the yearly averages. All are ICMEs, magnetic clouds mainly. For comparison with May 1998, we chose each event to be of 3-days' duration. This choice of duration has the added advantage of not discriminating against solar minimum events that tend to input considerable power in long-duration Alfvenic fluctuations on the fast stream which, at solar minimum, typically follows the ejecta [*Tsurutani and Gonzalez*, 1987; *Lepping et al.*, 1997; *Farrugia et al.*, 1998]. The events discussed are the following: 28–30 September 1978 (A), 13–15 January 1988 (B), 18–20 October 1995 (C), 27–29 May 1996 (D), 9–11 January 1997 (E), 1–3 May 1998 (F); 4 May 1998 (F′), 24–26 September 1998 (G), 6–8 April 2000 (H). With the possible exception of event H, all these events have been subject of intense study by the community principally because most were strongly geoeffective configurations. No other selection criteria have been applied except that the events chosen are well known to the community.

[40] The results of the comparison is shown in Figure 13. The top panel displays the calculated energy deposition, and the bottom panel displays the power averaged over 3 hours around peak power. Three hours are chosen for purposes of comparison with the period 0230– 0530 UT, 4 May. The horizontal arrow in the top panel shows the energy accumulated between 0230 and 0530 UT on 4 May 1998.

[41] A number of points are suggested by this data sample.

1. Over this solar cycle, there is a trend for the energy deposited by magnetic clouds to decrease toward minimum activity (approximately December 1996) and to increase with increasing solar activity. A similar trend may be seen in the maximum power deposited.

2. The energy appears to approach saturation at ~10 J

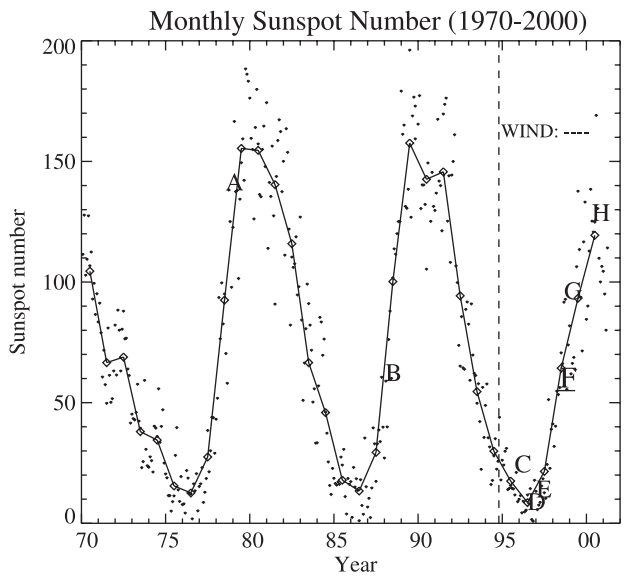

Figure 12. Distribution of events A–H with respect to the solar cycle. The monthly sunspot number (dots) for 1970–2000 and yearly averages (diamond symbols and joined by straight lines) are shown.

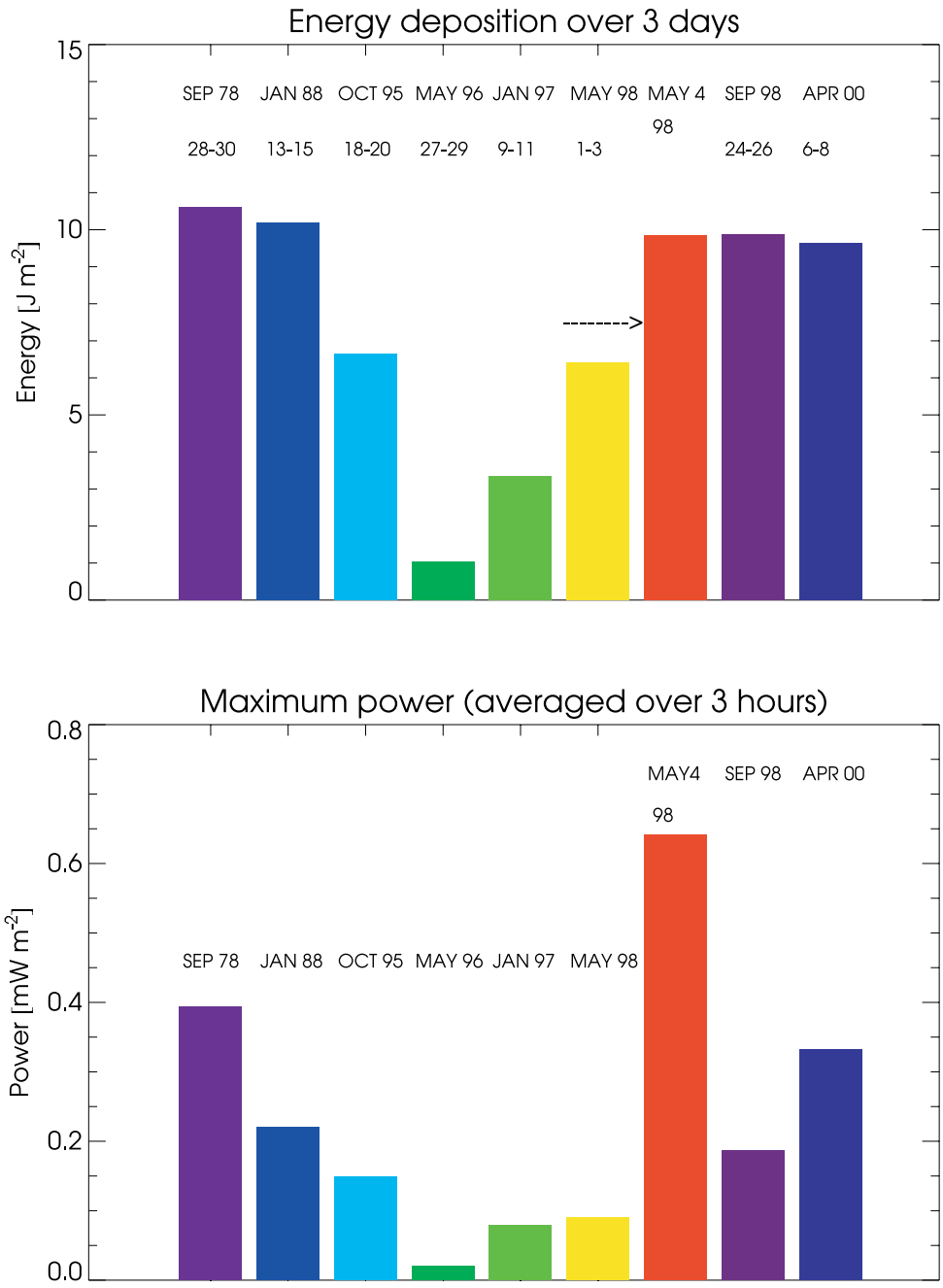

Figure 13. Predicted (top) energy and power to the magnetosphere during events A–H are compared with those on 4 May 1998.

m^{-2}; the maximum power, except on 4 May, approaches a value of ~0.4 mW m^{-2}. 3). The energy deposition on 4 May alone exceeds that on the preceding 3-day period, itself a very geoeffective interval, and the 3 hours on early 4 May account for ~75% of this;

3. The power on 4 May exceeds all the others by a factor >1.7. At a power of 0.64 mW m^{-2}, it clearly represents a large fluctuation from the norm, the average and standard deviation of the sample being 0.18 ± 0.13 mW m^{-2}. In summary, 4 May 1998 represented an unprecedented powering of the magnetosphere, exceeding all events during the rising phase of this solar cycle.

4. By implication, energy and power input of the 2–4 May 1998, configuration exceeded that of all the others in the sample by virtue of its being a compound stream. In the discussion we shall put these results on a firmer statistical foundation by considering the entire 6-year period 1995–2000, where continuous data coverage is available.

4. Discussion

[42] We examined interplanetary features of the period 1–4 May 1998, presenting new information on the field and

plasma structure, the shocks and discontinuites present, the magnetic connection of the ejecta to the Sun, and the electromagnetic power that one widely used formulation predicts the configuration to contain. May 1–4, 1998, formed part of the first prolonged interval of solar activity which culminated, as we have shown, in an unprecedented powering of the magnetosphere in a 3-hour burst early on 4 May. Data analyzed were from instruments on Wind, ACE, and SOHO and include iron and helium composition and charge state measurements, magnetic fields, and low and energetic protons and electrons.

4.1. Summary of Main Points

[43] The configuration consisted of a compound stream where a ICME was interacting with, and being overtaken by, a hot, very fast (900 km s^{-1}) stream. *Skoug et al.* [1999] have found that at the "core" of the configuration there is a magnetic cloud contained within an ICME. We followed this identification and that of the extent of the ejecta, and found the following:

1. The front boundary of the ICME is an RD.
2. The front edge of a hot, fast stream coincides with the rear boundary of the ICME. It has a zero normal field component, isolating the stream magnetically from the preceding ICME. Behind this interface, a very intense magnetic field is observed.
3. A shock is observed ahead of the ICME whose speed is comparable to that of the front edge of the ICME, consistent with its being driven by the ejecta.
4. A second shock occurs towards the rear end of the ejecta whose speed exceeds ambient values, consistent, in turn, with its overtaking the ejecta.
5. The hot, fast, noncorotating stream had the largest geoeffective potential of the whole 4 day period. Its leading edge affected the energetic particles even more strongly than the three shocks, which is probably related to the extreme magnetic field jump across it, by a factor of $\sim$4.
6. EPACT and EPAM fluxes show evidence of SEPs related to both gradual (shock) and implusive (flare) events.
7. Prompt onsets of solar energetic particles within the cloud during its earlier phase indicate that its "legs" were rooted to an active region on the Sun, based on an original idea by *Kahler and Reames* [1990]. Particles were sensed from different flares giving a lower limit to the size of the magnetic cloud's footprint for the first time.
8. During the second part of cloud passage over Wind (3 May) the solar wind halo population was extremely tenuous. This was probably partly responsible for the very cold core population since the halo is an important heating source for the core electron population [*Larson et al.*, 2000]. We suggested that this very tenuous halo is a result of scattering by Coulomb collisions whose frequency is enhanced by a combination of high density and low electron temperature. The tenuous halo coincided with the observation of unusual compositional signatures reported by other experimenters and ascribed to prominence material. There was a residual field-aligned component of the halo, however. The evidence for this is indirect, from the polar rain. The polar rain is believed to be due to precipitation of the field-aligned component of the solar wind electron halo (the strahl [*Fairfield and Scudder*, 1985]). Figure 14 shows Polar/Hydra measurements for 3 May. Plotted are the the magnetic latitude of the spacecraft; the differential energy fluxes of ions and electrons, with intensities according to the respective color bars on the right; the energy fluxes of electrons (red) and ions, integrated over pitch angle; and similarly integrated number fluxes. Positional information is given at bottom. On two successive crossings of the northern polar cap, centered at 0500 and 2100 UT, respectively, electron precipitation is measured up to energies of $\sim$600–700 eV. We note that with a sunward tilted IMF (see ϕ_B panel in Figure 1) the northern polar cap would usually be the unfavored hemisphere for polar rain and field lines threading the northern cap connect back to the Sun only because we have an ejecta passing Earth [*Gosling et al.*, 1986]. The residual collimation along the magnetic field may be due to the magnetic focussing as the electrons travel away from the Sun in a steadily decreasing magnetic field [*Lemons and Feldman*, 1983].
9. A huge powering of the magnetosphere is predicted on one formulation to result during the passage of the fast stream on 4 May, representing a large fluctuation from the norm. Comparing energy and power deposition to the magnetosphere by a set of very geoeffective configurations in a specific formulation (*Perreault and Akasofu*'s [1978] ϵ parameter), we find a systematic variation of both power and energy with solar cycle. Except for 4 May, both appear to saturate at $\sim$0.4 mW m^{-2} and 10 J m^{-1}, respectively.

4.2. RD at the Leading Edge of the ICME

[44] The front boundary of the ICME (D1) was shown to be a rotational discontinuity, based principally on the magnetic field. We think that the presence of an RD, and associated disturbances, at the leading edge of the ICME is consistent with the notion that the ICME started off with a TD at its front edge which then decayed through reconnection. Indeed, we found more structure consistent with this idea. We thus noted the presence of a magnetic hole and associated plasma heating and/or plasma acceleration at a structure in pressure balance. Magnetic depressions (holes) in the interplanetary medium have of course been examined by many people, but here we are concerned with a magnetic hole seen in association with a rotational discontinuity D1 near the front boundary of an ICME. This set of discontinuities may thus represent a reconnection layer. While the low resolution of the plasma data did not permit further detailed enquiry, a reconnection layer in interplanetary space composed of an RD and a magnetic hole has been analyzed in detail by *Farrugia et al.* [2001]. The magnetic hole was there shown to be a slow shock feature. Remote sensing disturbances (the reconnection is hardly likely to be local) from a distant X line opens interesting vistas for interplanetary research partly because the discontinuities have time to separate as they propagate to 1 AU at different speeds, but mainly because central problems in solar/interplanetary physics are predicated on the occurrence of reconnection. Thus, for example, *Gosling et al.* [1995] propose that the flux rope magnetic field topology of magnetic clouds might

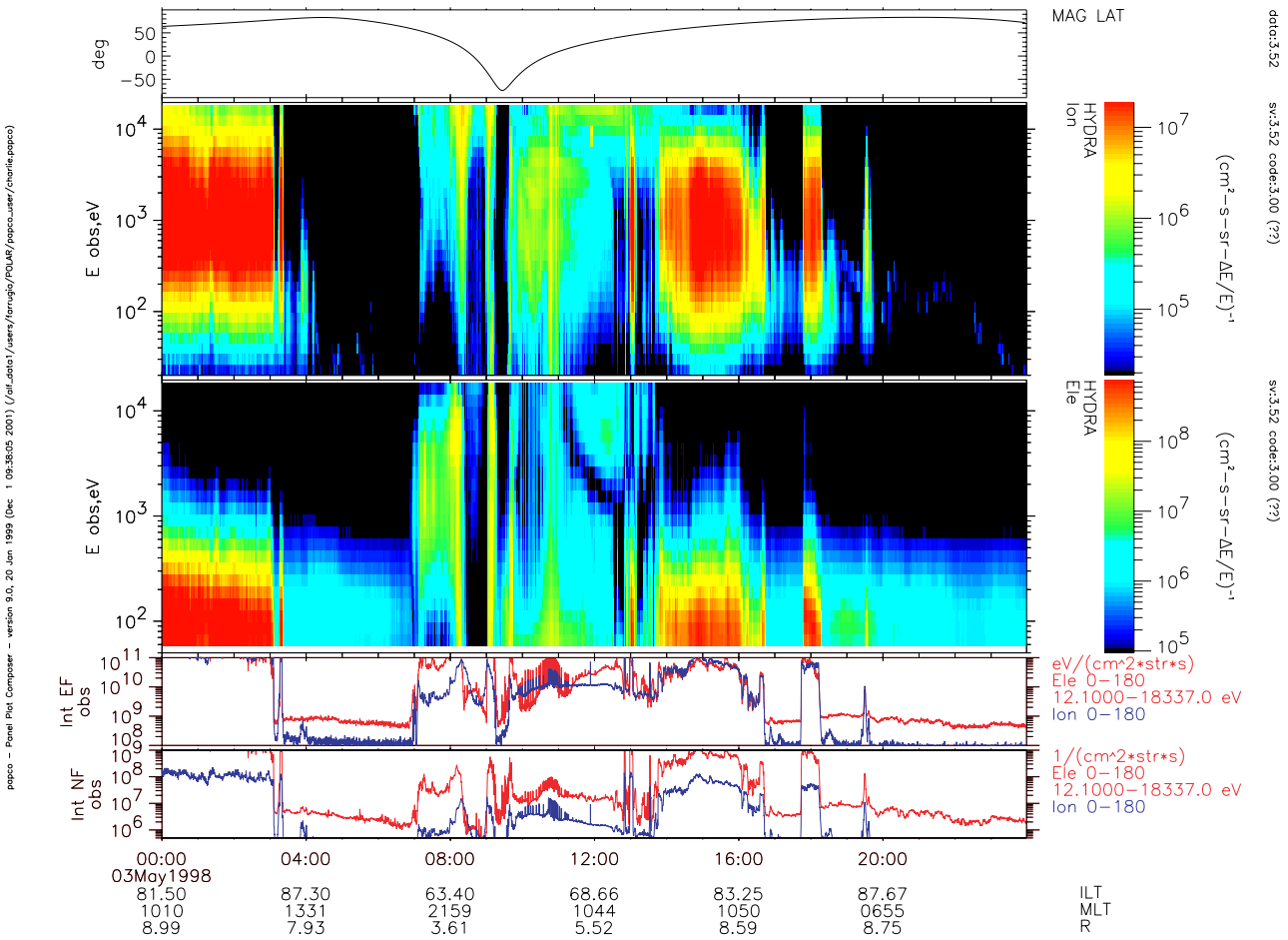

Figure 14. Polar/HYDRA measurements on 3 May 1998: (top to bottom) magnetic latitude of the spacecraft; differential energy fluxes of ions and electrons, with intensities according to the respective color bars on the right; energy fluxes of electrons (red) and ions, integrated over pitch angle; and similarly integrated number fluxes. Positional information is given at bottom. In two successive crossings of the northern polar cap, centered at 0500 and 2100 UT, respectively, the electron precipitation is measured up to energies of ~700 eV.

arise through reconnection processes close to the Sun. Another context is the long-standing problem of the disconnection of magnetic flux from the Sun [*Gosling*, 1975; *MacQueen*, 1980]. In this context, reconnection might be a means of disconnecting this flux, avoiding thereby a secular buildup of magnetic field strength at 1 AU, a circumstance that is not observed. There is plenty of scope for such studies, particularly when one keeps in mind the rich field of enquiry the early observations of reconnection at the magnetopause have given rise to.

[45] Three shocks were present in 30 April to 4 May 1998. As expected, energetic particle fluxes peaked at the shocks. Our observations of the behavior of SEPs near the leading edge of the high-speed stream suggest that a shock is sufficient but not necessary to produce SEPs. The degree of field increase appears to be the crucial parameter for energizing particles. A field compression occurs, of course, at shocks but it may also occur elsewhere. Thus the leading edge of this high-speed stream had a field compression ratio across it that is larger than that at the shocks.

4.3. Composition and Charge States

[46] Composition and charge state observations were an essential element of the investigation. The elemental and charge state composition of energetic particles provide a detailed phenomenology not only as regards the behavior at the shocks and field directional discontinuities forming part of the configuration but also as regards the relation of the interplanetary observations at 1 AU to solar events. In particular, they allowed us to infer connectivity to two separate flares which, in turn, provided a lower limit for the size of the magnetic cloud's solar footprint. Further, the Fe charge behavior gives us additional information on the structure of the cloud. Last, this behavior brings to light various acceleration mechanisms at the shocks and discontinuities, namely, (1) local shock acceleration, which may be

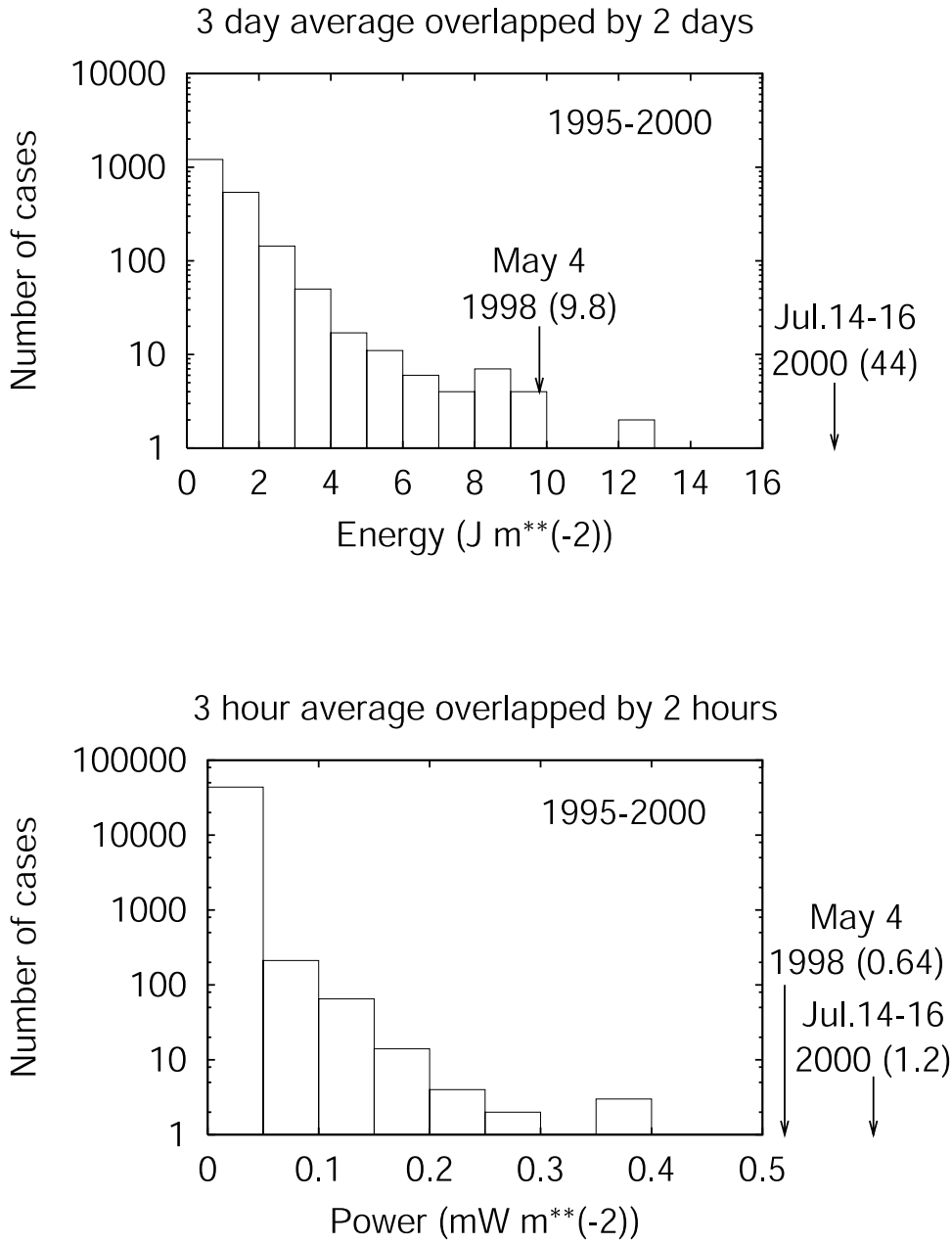

Figure 15. Histograms showing the frequency of occurrence of (top) energy and power, over 3 days and 3 hours, respectively, for the period 1995–2000, inclusive. The values attained on 4 May 1998 and 14–16 July 2000, indicated by arrows, are shown within parenthesis.

rigidity dependent [*Klecker et al.*, 2000]; (2) acceleration without a shock, and (3) flare-associated acceleration. For mechanism 2 the necessary observations for a full-scale modeling of these acceleration processes are present: solar wind charge states are available, though not shown here, as well as solar wind and IMF parameters and energetic particle charge states. The SEP production in the absence of a shock can thus be modeled, similar to what *Klecker et al.* [2000] did for shock S2.

[47] The SEPs observed during the strong magnetic field on 4 May offer an interesting comparison to those locally accelerated by the shock S2 on 1 May. The iron charge state distribution on 4 May extends to higher charge states than on 1 May. This may be a result of rigidity-dependent acceleration, but further modeling is needed to address this possibility.

4.4. Power and Energy Input: 1995–2000

[48] In terms of power and energy during the rising phase of this solar cycle, the 1–4 May event interrupted an otherwise smooth rise of power and energy. The comparisons made above on this topic were confined to a few examples, chosen because they represented strongly geo-effective configurations which are well known to the community. To place our comparisons of power and energy input to the magnetosphere on a firm statistical basis, we have examined the OMNI data for the 6-year period 1995–2000. Figure 15 shows the resulting histograms for energy

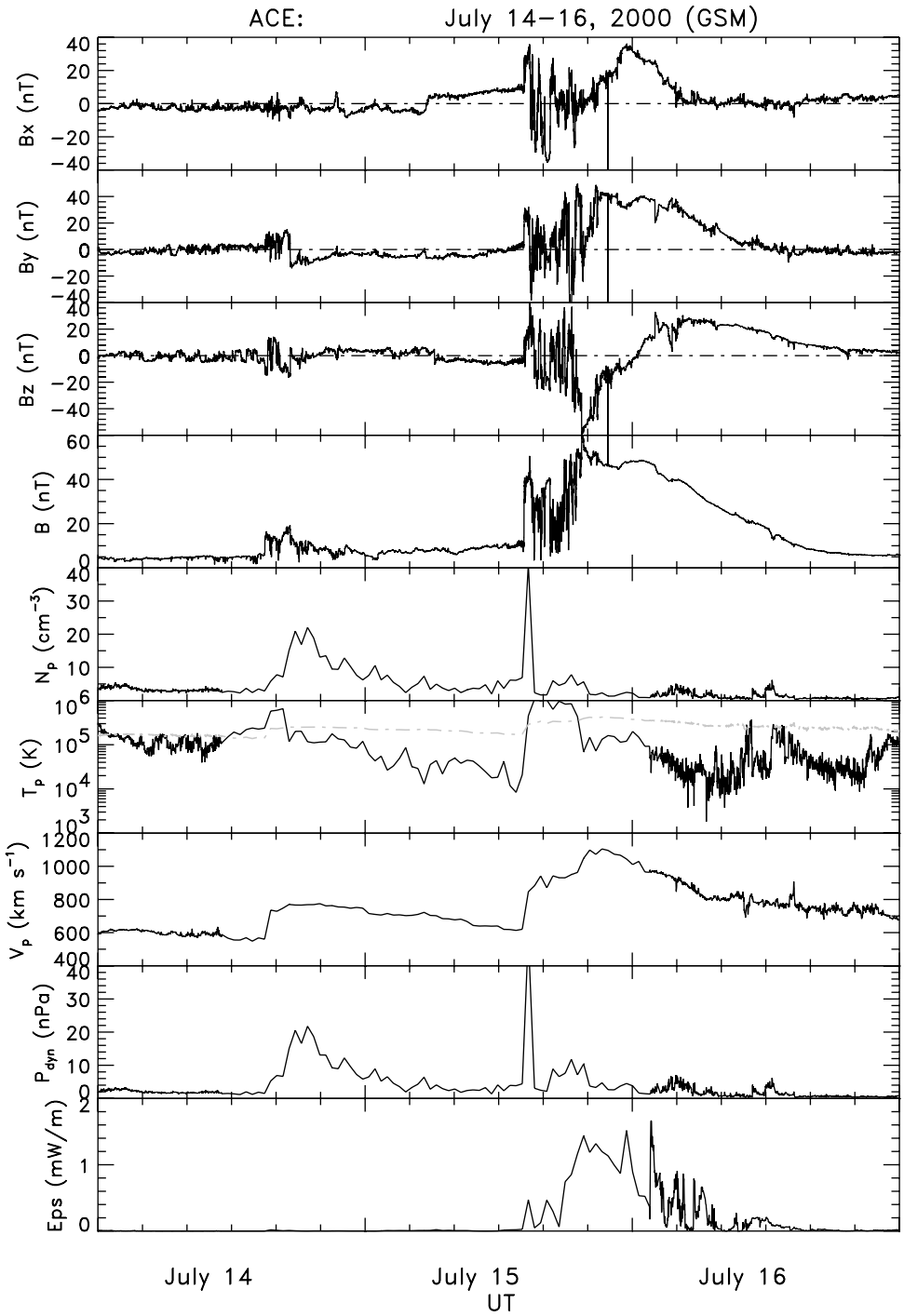

Figure 16. Proton and field parameters for 14–16 July 2000 ("Bastille day" event): (top to bottom) GSM components of the magnetic field, the total field, the proton density, temperature, and bulk speed, the dynamic pressure, and the ϵ parameter. Note the concentration of power during the $B_z < 0$ phase of magnetic cloud passage.

(top panel) and power. The data are running averages over 3 days and 3 hours, respectively, overlapped by two thirds. The top panel shows the frequency of occurrence of various values of the energy. The huge majority of intervals show an accumulation of <10 J m^{-2}, with 10 J m^{-2} appearing as an approximate upper bound. This is also the energy accumulated by 4 May 1998 in one day alone.

[49] The power input is shown in the second panel. Most 3-hour powers are < 0.3 mW m^{-2}, confirming our earlier findings. With 0.64 mW m^{-2} 4 May highlights the unprecedented power input during the erosion phase on 4 May.

[50] Though the compound stream overtook in power and energy all strongly geoeffective configurations seen since

1995, in neither is it the largest in this cycle. Using the same method as that for producing Figure 11, we have calculated the energy (over 3 days) and the average power near peak power (over 3 hours) for 14–16 July 2000 (the "Bastille Day" event). The 14–16 July 2000 field and plasma data are shown in Figure 16. The panels show from top to bottom the GSM components of the magnetic field, the total field, the proton density, temperature and bulk speed, the dynamic pressure and the epsilon parameter. On 15–16 July 2000, ACE observes a magnetic cloud, which drives a shock at ~15 UT, 15 July. In the sheath region, large-amplitude fluctuations in the north–south component, B_z, are evident. Within the magnetic cloud a large negative-to-positive excursion of the magnetic field occurs with a peak-to-peak amplitude of ~80 nT. The time series of the ϵ parameter in the bottom panel shows a large concentration of power occurring mostly during the passage sheath and the $B_z < 0$ phase of the ejecta. This contrasts with the 2–4 May 1998 event, where ϵ attains maximum values in the fast stream behind the ICME. A comparison of energy (over 3 days) and maximum power yields: 9.8 J versus 44.4 J m^{-2} (energy) and 0.65 versus 1.20 mW m^{-2} (power), i.e., on 16 July power peaks at twice the value on 4 May 1998, and the energy over 3 days is higher in July 2000 by a factor of ~3.

4.5. Geoeffectiveness of Compound Streams

[51] This work confirms the study of *Burlaga et al.* [1987] of the important role compound streams play in enhancing the geoeffective potential of ICMEs/magnetic clouds. Thus the largest storms studied in that work were due to compound streams. The arrival at Earth of the 2–3 May 1998 ICME caused major storm activity (min Dst ~ −100 nT), but the subsequent arrival of the high-speed stream made the Dst index plummet sharply to ~ −280 nT, converting a major into a great storm.

[52] The arrival at Earth of a strongly geoeffective, noncorotating stream on 4 May highlights a challenge to the space weather program, with its accent on monitoring ejecta, because it shows that, over and above the ejecta themselves, it is also the flows they run into en route to Earth, which can be of decisive importance in determining the resulting geoeffects. It also shows the importance of MHD modeling of the propagation of solar ejecta in the interplanetary medium. Still, the noncorotating nature of the 4 May stream might not be easy to predict and model. Perhaps the only advance signature at 1 AU would be the strong SEP enhancement which occurred at its leading edge.

[53] **Acknowledgments.** We are grateful to Ruth Skoug for provision of SWEPAM data. We thank Bernie J. Vasquez for helpful discussions and Jerry Needell for computational assistance. We are grateful to the referees for their very helpful suggestions, which improved the manuscript. We acknowledge the ACE SCIENCE CENTER and, in particular, the EPAM instrument team, PI Robert Gold, for provision of EPAM data, and P. I. Norman Ness for the ACE/MAG data. We also thank the EPACT team with PI T. T. von Rosenvinge. GOES data are courtesy of Solar Geophysical Data, US Department of Commerce, Boulder, CO, USA. We thank Robert P. Lin for the electron data from the 3-D Plasma Analyzer on WIND, through the CDA Web site. This work is supported by NASA Living with a Star grant NAG 5-10883, grants NAG5-2834, NAS5-32626, and NAG5-6912, and by DARA grant 50-OC-8911-0. The work at the University of Maryland was supported by NASA contract NAS5-30927 and grant NAG5-7228.

[54] Janet G. Luhmann thanks Victor J. Pizzo and Marcia Neugebauer for their assistance in evaluating this paper.

References

Abraham-Shrauner, B., and S. H. Yun, Interplanetary shocks seen by Ames plasma probe on Pioneer 6 and 7, *J. Geophys. Res.*, *81*, 2097, 1976.

Baker, D. N., S.-I. Akasofu, W. Baumjohann, J. W. Bieber, D. H. Fairfield, E. H. Hones Jr., B. Mauk, R. L. McPherron, and T. E. Moore, Substorms in the magnetosphere, in *Solar-Terrestrial Physics: Present and Future*, edited by D. M. Butler and K. Papadopoulos, *NASA Ref. Publ., 1120*, chap. 8, 1984.

Burke, W. J., D. R. Weimer, and N. C. Maynard, Geoeffective interplanetary scale sizes derived from regression analysis of polar cap potentials, *J. Geophys. Res.*, *104*, 9989, 1999.

Burlaga, L. F., E. Sittler Jr., F. Mariani, and R. Schwenn, Magnetic loop behind an interplanetary shock: Voyager, Helios and IMP 8 observations, *J. Geophys. Res.*, *86*, 6673, 1981.

Burlaga, L. F., K. W. Behannon, and L. W. Klein, Compound streams, magnetic clouds and major geomagnetic storms, *J. Geophys. Res.*, *92*, 5725, 1987.

Burlaga, L. F., R. P. Lepping, and J. Jones, Global configuration of a magnetic cloud, in *Physics of Magnetic Flux Ropes*, *Geophys. Monogr. Ser.*, vol. 58, edited by C. T. Russell, E. R. Priest, and L. C. Lee, p. 373, AGU, Washington, D. C., 1990.

Cane, H. V., I. G. Richardson, and G. Wibberenz, The response of energetic particles to the presence of ejecta material, *Proc. 24th Int. Cosmic Ray Conf.*, *4*, 377, 1995.

Fairfield, D. H., and J. D. Scudder, Polar rain: Solar coronal electrons in the Earth's magnetosphere, *J. Geophys. Res.*, *90*, 4055, 1985.

Farrugia, C. J., L. F. Burlaga, V. A. Osherovich, I. G. Richardson, M. P. Freeman, R. P. Lepping, and A. J. Lazarus, A study of an expanding interplanetary magnetic cloud and its interaction with the Earth's magnetosphere: The interplanetary aspect, *J. Geophys. Res.*, *98*, 7621, 1993a.

Farrugia, C. J., I. G. Richardson, L. F. Burlaga, V. A. Osherovich, and R. P. Lepping, Simultaneous observations of Solar MeV particles in a magnetic cloud and in the Earth's northern tail lobe: Implications for the global field line topology of magnetic clouds and entry of solar particles into tail lobe during cloud passage, *J. Geophys. Res.*, *98*, 15,497, 1993b.

Farrugia, C. J., N. V. Erkaev, H. K. Biernat, and L. F. Burlaga, Anomalous magnetosheath properties during Earth passage of an interplanetary magnetic cloud, *J. Geophys. Res.*, *100*, 19,245, 1995.

Farrugia, C. J., L. F. Burlaga, and R. P. Lepping, Magnetic clouds and the quiet-storm effect at Earth, in *Magnetic Storms*, edited by B. T. Tsurutani, W. D. Gonzalez, Y. Kamide, and J. K. Arballo, p. 91, *Geophys. Res. Monograph. Series, 98*, AGU, Washington, D. C., 1997.

Farrugia, C. J., J. D. Scudder, and M. P. Freeman, et al., Geoeffectiveness of three Wind magnetic clouds: A comparative study, *J. Geophys. Res.*, *103*, 17,261, 1998.

Farrugia, C. J., B. J. Vasquez, I. G. Richardson, et al., A reconnection layer associated with a magnetic cloud, *Adv. Space Res.*, *28*(5), 759, 2001.

Freeman, M. P., and C. J. Farrugia, Solar wind input between substorm onsets during and after the October 18–20, 1995, magnetic cloud, *J. Geophys. Res.*, *104*, 22,729, 1999.

Gloeckler, G., et al., Investigation of the composition of solar and interstellar matter using solar wind and pick-up ion measurements with SWICS and SWIMS on the ACE spacecraft, *Space Sci. Rev.*, *86*, 497, 1998.

Gloeckler, G., L. A. Fisk, and S. Hefti, et al., Unusual composition of the solar wind in the 2–3 May 1998 CME observed with SWICS on ACE, *Geophys. Res. Lett.*, *26*, 157, 1999.

Gold, R. E., et al., Electron, Proton, and Alpha Monitor on the Advanced Composition Explorer Spacecraft, *Space Sci. Rev.*, *86*, 541, 1998.

Gosling, J. T., Large-scale inhomgeneities in the solar wind of solar origin, *Rev. Geophys.*, *13*, 1053, 1975.

Gosling, J. T., Coronal mass ejections and magnetic flux ropes in interplanetary space, in *Physics of Magnetic Flux Ropes*, edited by C. T. Russell, E. R. Priest, and L. C. Lee, p. 344, *Geophysical Monogr.*, vol. 58, AGU, 1990.

Gosling, J. T., V. Pizzo, and S. J. Bame, Anomalously low proton temperatures in the solar wind following interplanetary shocks: Evidence for magnetic bottles?, *J. Geophys. Res.*, *78*, 2001, 1973.

Gosling, J. T., D. N. Baker, S. J. Bame, and R. D. Zwickl, Bidirectional solar wind electron heat flux adn hemispherically symmetric polar rain, *J. Geophys. Res.*, *91*, 11,352, 1986.

Gosling, J. T., D. N. Baker, S. J. Bame, et al., Bidirectional solar wind electron heat flux events, *J. Geophys. Res.*, *92*, 8519, 1987.

Gosling, J. T., S. J. Bame, D. J. McComas, and J. L. Phillips, Coronal mass ejections and large geomagnetic storms, *Geophys. Res. Lett.*, *17*, 901, 1990.

Gosling, J. T., D. J. McComas, J. L. Phillips, and S. J. Bame, Geomagnetic activity associated with Earth passage of interplanetary shock disturbances and coronal mass ejections, *J. Geophys. Res.*, *96*, 7831, 1991.

Gosling, J. T., J. Birn, and M. Hesse, Three-dimensional magnetic reconnection and the magnetic topology of coronal mass ejections, *Geophys. Res. Lett.*, *22*, 869, 1995.

Isenberg, P. A., The solar wind, in *Geomagnetism*, vol. 4, edited by J. A. Jacobs, pp. 1–88, Academic, San Diego, Calif., 1991.

Kahler, S. W., and D. V. Reames, Solar energetic particles as probes of the structure of magnetic clouds, *Proc. Int. Cosmic Ray Conf. 21st*, *5*, 245, 1990.

Kan, J. R., and L. C. Lee, Energy coupling function and solar wind-magnetospheric dynamo, *Geophys. Res. Lett.*, *6*, 577, 1979.

Klecker, B., et al., Comparison of ionic charge states of energetic particles with solar wind charge states in CME related events, paper presented at ACE-2000 Symposium Proceedings, Am. Inst. of Phys., New York, 2000.

Klein, L. W., and L. F. Burlaga, Interplanetary magnetic clouds at 1 AU, *J. Geophys. Res.*, *87*, 613, 1982.

Larson, D. E., R. P. Lin, and J. Steinberg, Extremely cold electrons in the January 1997 magnetic cloud, *Geophys. Res. Lett.*, *27*, 157, 2000.

Lemons, D. S., and W. C. Feldman, Collisional modification to the exospheric theory of solar wind halo electron pitch angle distributions, *J. Geophys. Res.*, *88*, 6881, 1983.

Lepping, R. P., and K. W. Behannon, Magnetic field directional discontinuities, 1, Minimum variance errors, *J. Geophys. Res.*, *85*, 4695, 1980.

Lepping, R. P., et al., The WIND magnetic field investigation, *Space Sci. Rev.*, *71*, 207, 1995.

Lepping, R. P., et al., The WIND magnetic cloud and events of October 18–20, 1995: Interplanetary properties and as triggers for geomagnetic activity, *J. Geophys. Res.*, *102*, 14,049, 1997.

Lin, R. P., and S. W. Kahler, Interplanetary magnetic field connection to the Sun during electron heat flux dropouts in the solar wind, *J. Geophys. Res.*, *97*, 8203, 1992.

Lin, R. P., et al., A three-dimensional plasma and energetic particle investigation for the Wind spacecraft, *Space Sci. Rev.*, *71*, 125, 1995.

Lopez, R. E., Solar cycle invariance in solar wind proton temperature realtionships, *J. Geophys. Res.*, *92*, 11,189, 1987.

Lu, G., D. N. Baker, R. L. McPherron, C. J. Farrugia, V. K. Jordanova, et al., Global energy deposition during the January 1997 magnetic cloud event, *J. Geophys. Res.*, *103*, 11,685, 1998.

Luhn, A., B. Klecker, D. Hovestadt, and E. Möbius, The mean charge of silicon in ^{3}He-rich solar flares, *Astrophys. J.*, *317*, 951, 1987.

MacQueen, R. M., Coronal transients: A summary, *Philos. Trans. R. Soc. London, Ser. A*, *207*, 605, 1980.

Möbius, E., et al., The solar energetic particle ionic charge analyzer (SEPICA) and the data processing unit (S3DPU) for SWICS, SWIMS, and SEPICA, *Space Sci. Rev.*, *86*, 449, 1998.

Ogilvie, K. W., et al., SWE, A comprehensive plasma instrument for the WIND spacecraft, *Space Sci. Rev.*, *71*, 55, 1995.

Paschmann, G., et al., The magnetopause for large magnetic shear: AMPTE/IRM observations, *J. Geophys. Res.*, *91*, 11,099, 1986.

Perreault, P., and S.-I. Akasofu, A study of geomagnetic storms, *Geophys. J. R. Astron. Soc.*, *54*, 547, 1978.

Popecki, M. A., et al., Simultaneous high Fe charge state measurements by solar energetic particle and solar wind instruments, paper presented at ACE-2000 Symposium Proceedings, Am. Inst. of Phys., New York, 2000.

Reames, D. V., Particle acceleration at the Sun and in the heliosphere, *Space Sci. Rev.*, *90*(3/4), 413, 1999.

Reiff, P. H., R. W. Spiro, and T. W. Hill, Dependence of polar cap potential on interplanetary parameters, *J. Geophys. Res.*, *86*, 7639, 1981.

Richardson, I. G., C. J. Farrugia, and L. F. Burlaga, Energetic observations in the magnetic cloud of 14–15 January 1988 and their implications for the magnetic field, *Proc. 22nd Int. Cosmic Ray Conf.*, *3*, 597, 1991.

Richardson, I. G., Using energetic particles to probe the magnetic topology of ejecta, in *Coronal Mass Ejections*, *Geophys. Monogr. Ser.*, vol. 99, edited by N. U. Crooker et al., p. 189, AGU, Washington, D. C., 1997.

Richardson, I. G., and H. V. Cane, Regions of abnormally low proton temperatures in the solar wind (1965–1991) and their association with ejecta, *J. Geophys. Res.*, *100*, 23,397, 1995.

Richardson, I. G., H. V. Cane, and T. T. von Rosenvinge, Prompt arrival of solar energetic particles from far eastern events: The role of large-scale interplanetary magnetic field structure, *J. Geophys. Res.*, *96*, 7853, 1991.

Richardson, I. G., E. W. Cliver, and H. V. Cane, Sources of geomagnetic activity over the solar cycle: Relative importance of coronal mass ejections, high-speed streams, and slow solar wind, *J. Geophys. Res.*, *105*, 18,203, 2000.

Skoug, R. M., et al., A prolonged He^+ enhancement within a coronal mass ejection in the solar wind, *Geophys. Res. Lett.*, *26*, 161, 1999.

Sonnerup, B. U. Ö., The reconnecting magnetosphere, in *Magnetospheric Physics*, edited by B. M. McCormac, p. 23, D. Reidel, Norwell, Mass., 1974.

Sonnerup, B. U. Ö., and L. J. Cahill, Magnetopause structure and attitude from Explorer 12 observations, *J. Geophys. Res.*, *72*, 171, 1967.

Tsurutani, B. T., and W. D. Gonzalez, The cause of high-intensity long-duration continuous AE activity (HILDCAAs): Interplanetary Alfven wave trains, *Planet. Space Sci.*, *35*, 405, 1987.

Tsurutani, B. T., and W. D. Gonzalez, The interplanetary causes of magnetic storms: A review, in *Magnetic Storms*, *Geophys. Monogr. Ser.*, vol. 98, edited by B. T. Tsurutani et al., p. 77, AGU, Washington, D. C., 1997.

Tsurutani, B. T., et al., Origin of interplanetary southward magnetic fields responsible for major magnetic storms near solar maximum (1978–1979), *J. Geophys. Res.*, *93*, 8519, 1988.

von Rosenvinge, T. T., et al., The Energetic Particles: Acceleration, Composition, and Transport (EPACT) Investigation on the Wind spacecraft, *Space Sci. Rev.*, *71*, 155, 1995.

Zhang, G., and L. F. Burlaga, Magnetic clouds, geomagnetic disturbances and cosmic ray decreases, *J. Geophys. Res.*, *95*, 2511, 1988.

L. F. Burlaga, R. D. Fitzenreiter, G. R. Lawrence, R. P. Lepping, and K. W. Ogilvie, NASA Goddard Space Flight Center, Greenbelt, MD 20771, USA.

M. I. Desai and G. M. Mason, Department of Physics, University of Maryland, College Park, MD 20771, USA.

J. R. Dwyer, Florida Institute of Technology, Physics and Space Sciences Department, Melbourne, FL 32901, USA.

C. J. Farrugia, V. K. Jordanova, H. Matsui, E. Möbius, J. Needell, and M. Popecki, Space Science Center, University of New Hampshire, Durham, NH 03824, USA. (charlie.farrugia@unh.edu)

D. McComas, Southwest Research Institute, San Antonio, TX 78228, USA.

S. Lepri and T. Zurbuchen, Space Research Building, University of Michigan, Ann Arbor, MI 48109, USA.